Minimum Speed Seeking Control for Nonhovering Autonomous Underwater Vehicles

You Hong Eng and Mandar Chitre
ARL, Tropical Marine Science Institute, National University of Singapore, Singapore
e-mail: youhong.eng@gmail.com, mandar@nus.edu.sg
Kien Ming Ng and Kwong Meng Teo
Department of Industrial & Systems Engineering, National University of Singapore, Singapore
e-mail: kienming@nus.edu.sg, kwongmeng@nus.edu.sg

Received 14 November 2014; accepted 15 July 2015

Most autonomous underwater vehicles (AUVs) are propelled by a single thruster, use elevators and rudders as control surfaces, and are torpedo-shaped. Furthermore, they are positively buoyant to facilitate recovery during an emergency. For this class of nonhovering AUVs, there is a minimum speed at which the AUV must travel for stable depth control. Otherwise, the extra buoyancy will bring the AUV up to the surface when the fin loses its effectiveness at low speeds. Hence, we develop a novel algorithm such that the AUV is automatically controlled to travel at its minimum speed while maintaining a constant depth. This capability is important in a number of practical scenarios, including underwater loitering with minimum energy consumption, underwater docking with minimum impact, and high-resolution sensing at minimum speed. First, we construct a depth dynamic model to explain the mechanism of the minimum speed, and we show its relationship with the buoyancy, the righting moment, and the fin's effectiveness of the AUV. Next, we discuss the minimum speed seeking problem under the framework of extremum seeking. We extend the framework by introducing a new definition of steady-state mapping that imposes new structure on the seeking algorithm. The proposed algorithm employs a fuzzy inference system, which is driven by the real-time measurements of pitch error and elevator deflection. The effectiveness of the algorithm in seeking the minimum speed is validated in both simulations and field experiments. © 2015 Wiley Periodicals, Inc.

1. INTRODUCTION

The oceans cover 71% of the earth's surface, and they play an important role in the planet's climate and weather systems. However, many scientific investigations of the oceans are hindered by the lack of samples in both space and time. It is believed that unmanned underwater vehicles (UUVs), which are one of the emerging technologies, will be able to change the landscape of the decade-long problem of undersampled oceans.

Broadly speaking, there are two classes of UUVs: remotely operated vehicles (ROVs) and autonomous underwater vehicles (AUVs). ROVs are tethered vehicles with umbilical cables that transfer power, sensor data, and control commands between the surface ship and the vehicles. They are teleoperated by human pilots and hence can perform complicated tasks such as underwater structure installations. As they enjoy an unlimited power source from a surface ship, ROVs usually have an open frame design and are equipped with multithrusters for greater maneuvering capability. On the other hand, AUVs are *tetherless* vehicles, and they have to carry their own onboard energy source. Due to the limited energy supply, AUVs are usually designed to have a streamlined shape (torpedo-like) in order to reduce drag. They are often propelled by a single thruster, and they maneuver via multiple control fins. As the number of actuators is less than the degrees of freedom (DoFs), AUVs are underactuated. In contrast to ROVs, AUVs are more mobile, and they can be used to survey a large area in a shorter period of time. Hence, they are the main workhorses for oceanographic surveys, sampling, and monitoring.

With continuous advances in technology, in terms of both software and hardware, AUVs have become commercially available for ocean exploration. Some commonly known AUVs include *Gavia* AUV (Teledyne Technologies Incorporated, 2014), *Iver* AUV (OceanServer, 2014), and *REMUS* AUV (Kongsberg Maritime, 2014). They are very similar in terms of dynamics and control. They are propelled by a single thruster, use elevators and rudders as control surfaces, and are torpedo-shaped. One central problem common to this class of nonhovering AUVs is their difficulty in performing low-speed maneuvers.

Direct correspondence to tmseyh@nus.edu.sg

 © 2015 Wiley Periodicals, Inc.
View this article online at wileyonlinelibrary.com • DOI: 10.1002/rob.21625

Nonhovering AUVs are controlled by fins, which lose their effectiveness at low speeds. Hence, there is a minimum speed at which the AUV must travel before losing its maneuvering capability. Traveling at low speeds is desired in a number of practical scenarios. An AUV consumes less energy when it travels slowly, thus maximizing endurance.[1] This contributes greatly to the long-term deployment of the AUV in environmental monitoring applications. The second scenario occurs when the AUV needs to perform underwater docking for battery charging and data transmission. In this case, the AUV should travel as slowly as possible so that the mechanical impact on the docking system is minimized. As pointed out by LeBas (1997), traveling slowly also improves the final homing maneuver effectiveness. The third scenario happens when the AUV is required to conduct close observations of particular areas of interest, such as mines, coral reefs, and offshore installations. For example, in the case of sidescan sonar, the slower the AUV travels, the more scanlines can be acquired from the same target, which gives a higher image resolution.

The potential benefits of operating the AUV at low speeds have attracted a number of researchers. Liu et al. (2009) improved the low-speed maneuverability of the *Delphin* AUV by adding four thrusters to provide hovering capability to the AUV. In his Master's thesis, Helgason (2012) examined ways to overcome the limitation that requires the *Gavia* AUV to cruise at speeds above 1.5 m/s. He focused on deriving the equation of motion for the AUV when external thrusters are attached to excite the respective DoF (surge, sway, heave, and yaw). In Nickell, Woolsey, and Stilwell (2005), the authors investigated the use of a moving mass actuator to augment the existing fins to achieve a lower minimum speed. In the Master's thesis of LeBas (1997), a new robust controller was proposed to handle the change of the hydrodynamic characteristic when the speed is varied. Furthermore, a speed-dependent pitch limit was introduced so that the stall condition at low speed could be avoided.

In Nickell (2005), the author derived the minimum speed based on the mass, the equilibrium angle of attack, and some other hydrodynamic coefficients of the AUV. However it is not easy to find the exact minimum speed, as the hydrodynamic coefficients are generally unknown. In addition to hydrodynamic characteristics, the minimum speed attainable by an AUV is also affected by the disturbances from its surroundings. Therefore, any prior determination of the minimum speed via trial and error would be either highly conservative or else it runs the risk of the AUV losing its controllability. Furthermore, for each deployment, the vehicle dynamics could be affected by the changes in payload configuration or trimming conditions [buoyancy and center of gravity (CG)]. Finding the new minimum speed for each deployment via trial and error would take too much effort and is thus not practical. Therefore, an algorithm that automatically tracks the minimum speed in real-time is desirable, so that the minimum vehicle speed can adapt to the changes in the AUV and the environment.

The minimum speed of the AUV should be defined in terms of its relative speed to the surrounding water instead of the ground speed. First, it is the relative speed that determines the hydrodynamic forces acting on the vehicle body and fins. Second, minimizing the AUV speed in terms of ground speed should be avoided because the ground speed is affected by underwater currents and requires instrumentation in the form of a Doppler Velocity Log (DVL), which is an expensive sensor and not all AUVs are equipped with it. The AUV's relative speed to the surrounding water is purely a function of AUV thrust. Hence, instead of minimizing speed, we solve the equivalent problem of minimizing thrust ratio, which is invariant under the influence of the underwater current.

In this paper, we aim to introduce new behavior to the class of nonhovering AUVs: while the AUV maintains a certain depth and heading, its cruising speed is continuously regulated in real-time to its minimum. To the best of our knowledge, such behavior is totally new and has not been developed previously. We require minimum speed when we want minimum energy consumption, minimum impact when docking the AUV, and slowest passage over the target of interest. From the simulation studies and experimental results, we find that the proposed minimum speed seeking algorithm is robust to changes in vehicle dynamics as well as environmental disturbances. We recommend implementation of the algorithm on existing AUVs, and we hope that this will open up new possibilities in the operation and application of AUVs.

The key contributions of this paper are (1) the formulation of the problem of minimum speed seeking for nonhovering AUVs, (2) mathematical modeling of the AUV depth dynamics to explain the mechanism of the minimum speed and its properties, (3) a novel minimum speed seeking algorithm and simulation studies of its performance, and (4) experimental verification of the proposed algorithm in the field with the *STARFISH* AUV.

This paper is organized as follows. First, a model of depth dynamics of an AUV is developed in Section 2. In Section 3, we explain the mechanism of minimum speed and show how it can be calculated under the modeling framework. We investigate the characteristics of the AUV when it cruises below its minimum speed. Based on its characteristics, we design the minimum speed seeking algorithm in Section 4. Simulation and experimental results are presented in Sections 5 and 6, respectively. Lastly, the concluding remarks are made in Section 7.

[1] Maximum endurance is not equivalent to maximum range. Maximum range is a function of the vehicle's speed and the hotel load. However, as pointed out by Singh, Yoerger, and Bradley (1997), range is generally maximized by reducing both the hotel load as well as the vehicle's speed.

2. AUV MODEL—DIVE PLANE

In this section, the dynamical model of a streamline, tail-controlled AUV is constructed by restricting the motion of the AUV to the dive-plane. By deriving the dynamic model, we try to understand the underlying interaction of forces and moments, and thus the mechanism behind the existence of the minimum speed. The model is also used later in a simulation to study the performance of the proposed minimum speed seeking algorithm.

Dynamic modeling of the underwater vehicle can be found throughout the literature (Abkowitz, 1969; Fossen, 1994; Healey & Lienard, 1993). Here, we adopt the model developed by Petrich, Neu, and Stilwell (2007), in which the equations of motion are written in the stability-axis frame of the AUV. This enables the hydrodynamic forces and moments to be more conveniently expressed.

Figure 1 shows three reference frames that are used to describe the motion of the AUV. They are labeled in green. First, the body-axis frame is centered at the vehicle center of buoyancy (CB) and the x_b axis is running along the longitudinal axis of symmetry, with positive pointing toward the vehicle's nose. The y_b axis is pointing at the starboard side of the AUV, and the z_b axis, which is orthogonal to both x_b and y_b, is pointing toward the bottom of the vehicle. Second, the inertia-axis frame is defined by pointing the Z with the gravitational force and aligning the Y with y_b. Finally, the stability-axis frame has its x_v axis placed along the vehicle velocity, aligning y_v with y_b. The body-axis and inertia-axis frame are related through a rotation about the common y axis with the pitch angle θ, whereas the body-axis and stability-axis frame are related through the angle of attack α about the same y axis. According to the defined frames, θ is positive when the AUV is upward pitching and negative when it is downward pitching. A similar sign convention applies for α as well.

We assume sway velocity v and vehicle roll ϕ to be zero. This is in agreement with the widely used decoupled assumption for streamlined AUVs (Healey & Lienard, 1993; Jalving, 1994). We are interested in modeling the vehicle states: depth Z, vehicle speed V, angle of attack α, pitch θ, and pitch rate q, given the elevator deflection δ and thruster force F_t as the inputs.

2.1. Kinematics

From a kinematics analysis of Figure 1, the rate of change of depth, $\dot{z}$, is

$$\dot{z} = V[-\cos\alpha\sin\theta + \sin\alpha\cos\theta]. \tag{1}$$

The vehicle speed V is related to body-axis surge velocity u and heave velocity w as

$$u = V\cos\alpha \quad \text{and} \quad w = V\sin\alpha. \tag{2}$$

The vehicle speed V is the speed relative to the surrounding water, which determines the hydrodynamic forces acting on the vehicle body and fins. Thus, it is invariant under the effect of underwater current. On the other hand, the vehicle ground speed, which is the resultant of vehicle speed V and underwater current, is affected by the current.

2.2. Equations of Motion

From Petrich et al. (2007), the equations of motion containing state vector $\mathbf{x} = [V, \alpha, q, \theta]$ and input $\mathbf{u} = [\delta, F_t]$ can be written as

$$\mathbf{ET}(\mathbf{x})\dot{\mathbf{x}} = \mathbf{R}(\mathbf{x}) + \mathbf{F}(\mathbf{x}, \mathbf{u}). \tag{3}$$

The transformation matrix $\mathbf{T}(\mathbf{x})$ is given by

$$\mathbf{T}(\mathbf{x}) = \begin{pmatrix} \cos\alpha & -V\sin\alpha & 0 & 0 \\ \sin\alpha & V\cos\alpha & 0 & 0 \\ 0 & 0 & 1 & 0 \\ 0 & 0 & 0 & 1 \end{pmatrix} \tag{4}$$

and the inertia matrix $\mathbf{E}$ is given by

$$\mathbf{E} = \begin{pmatrix} m_x & 0 & mz_{cg} & 0 \\ 0 & m_z & -mx_{cg} & 0 \\ mz_{cg} & -mx_{cg} & J_y & 0 \\ 0 & 0 & 0 & 1 \end{pmatrix}. \tag{5}$$

The right-hand side terms are

$$\mathbf{R}(\mathbf{x}) = \begin{pmatrix} -m_z qV\sin\alpha - mx_{cg}q^2 \\ m_x qV\cos\alpha + mz_{cg}q^2 \\ (m_z - m_x)V^2\cos\alpha\sin\alpha - m(x_{cg}\cos\alpha + z_{cg}\sin\alpha)qV \\ q \end{pmatrix} \tag{6}$$

and

$$\mathbf{F}(\mathbf{x}, \mathbf{u}) = \begin{pmatrix} F_x(\mathbf{x}, \mathbf{u}) \\ F_z(\mathbf{x}, \mathbf{u}) \\ M_y(\mathbf{x}, \mathbf{u}) \\ 0 \end{pmatrix}, \tag{7}$$

where m is the dry mass of the vehicle. m_x and m_z denote the dry mass plus added mass in the surge and heave direction, respectively. The vehicle's moment of inertia around the pitch axis including the added moment of inertia is J_y. The distance vector from the center of gravity to the center of buoyancy is $\mathbf{r}_{cg} = [x_{cg} \;\; y_{cg} \;\; z_{cg}]$.

External forces and moments are of the form

$$F_x(\mathbf{x}, \mathbf{u}) = \cos\alpha F_D(V, \alpha, \delta) - \sin\alpha F_L(V, \alpha, \delta) - (F_W - F_B)\sin\theta + F_t, \tag{8}$$

$$F_z(\mathbf{x}, \mathbf{u}) = \sin\alpha F_D(V, \alpha, \delta) + \cos\alpha F_L(V, \alpha, \delta) + (F_W - F_B)\cos\theta, \tag{9}$$

$$M_y(\mathbf{x}, \mathbf{u}) = M_q(V, \alpha, q, \delta) - (x_{cg}\cos\theta + z_{cg}\sin\theta)F_w. \tag{10}$$

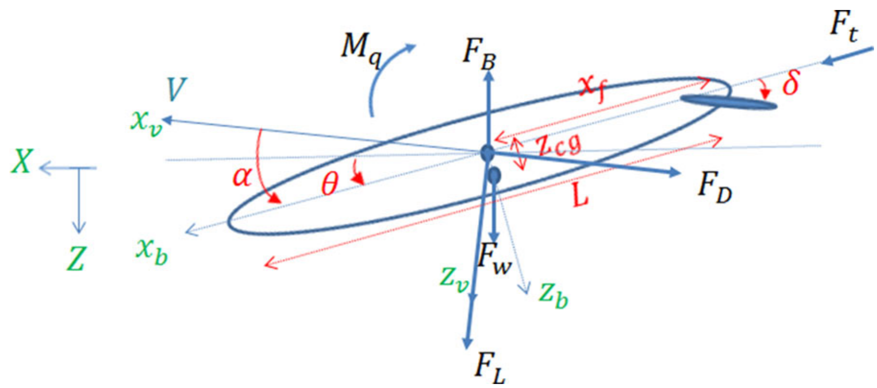

Figure 1. Free body diagram in the dive-plane.

F_w and F_B are the vehicle's weight and buoyancy forces, respectively. The extra buoyancy is calculated by finding the difference between the weight and buoyancy ($F_w - F_B$). The last term in Eq. (10), $(x_{cg}\cos\theta + z_{cg}\sin\theta)F_w$, is the hydrostatic righting moment. Thrust force is denoted as F_t. The hydrodynamic drag, lift force, and pitch moment generated by the vehicle's body and fins are $F_D(V,\alpha,\delta)$, $F_L(V,\alpha,\delta)$, and $M_q(V,\alpha,q,\delta)$, respectively. They are modeled as follows:

$$F_D(V,\alpha,\delta) = \frac{1}{2}\rho V^2 A_b C_{D_0}, \tag{11}$$

$$F_L(V,\alpha,\delta) = \frac{1}{2}\rho V^2\{A_b C_{L_\alpha}\alpha + A_f C_{L_\delta}\delta\}, \tag{12}$$

$$M_q(V,\alpha,q,\delta) = \frac{1}{2}\rho V^2\{A_b L[C_{m_\alpha}\alpha + C_{m_q}q] + A_f x_f C_{L_\delta}\delta\}. \tag{13}$$

ρ is the water density. A_b and A_f are the reference surface area for the body and fins, respectively. L is the reference length of the vehicle, whereas x_f is the distance between the fins and the center of buoyancy (see Figure 1). The hydrodynamic coefficients for drag, body lift, and fins lift are C_{D_0}, C_{L_α}, and C_{L_δ}, respectively. As for pitch moment, the hydrodynamic coefficient C_{m_α} accounts for the body's restoring moment, and C_{m_q} accounts for the viscous damping.

2.3. Maximum Elevator Deflection, δ_{max}

A typical lift curve is shown in Figure 2 for the NACA-0012 fin profile. From zero deflection, the coefficient of lift increases with the elevator deflection. The trend continues up to a critical angle, also known as the fin stall angle, which produces maximum lift coefficient. Beyond this critical angle, the laminar flow separates from the surface of a fin. At this region, the drag coefficient increases drastically with increasing deflection angle, but the lift coefficient falls rapidly with increasing deflection angle. Hence, the AUV is said to be in a stall condition when the elevator operates above the fin stall angle, δ_{stall}.

According to the lift equation, Lift L produced by a fin is equal to the lift coefficient C_L times the density ρ times half of the velocity V squared times the wing area A_f,

$$L = \frac{1}{2}A_f C_L \rho V^2. \tag{14}$$

As the C_L varies linearly with the elevator deflection δ, the lift coefficient is approximated as

$$C_L = C_{L_\delta}\delta, \tag{15}$$

where C_{L_δ} is the slope of the lift curve (Figure 2). This gives rise to the lift force generated by fins in Eq. (12).

Most controller designs require the fins to work within the linear region, and thus fin stall has to be avoided. Hence, we introduce a saturation block that sets the maximum elevator deflection from the pitch controller to δ_{max} (see Figure 3). The value of δ_{max} is normally chosen to be less than or equal to δ_{stall}.

2.4. Thruster Model

In this paper, we normalize the thrust force F_t into a scale from 0 to 1, and it is denoted as the thrust ratio T_R. The relationship between T_R and the actual thrust force produced by the thruster is shown in Figure 4. There is a dead zone from 0 to 0.28 where no thrust is generated. From 0.28 onward, the thrust force increases quadratically with the thrust ratio as shown by Figure 4,

$$F_t = 120T_R^2 - 31T_R + 0.53. \tag{16}$$

Equation (16) is obtained by best fitting the quadratic equation on the measurements made by the thruster manufacturer. The value 0.28 is obtained at the intersection between the best fit curve and the x axis.

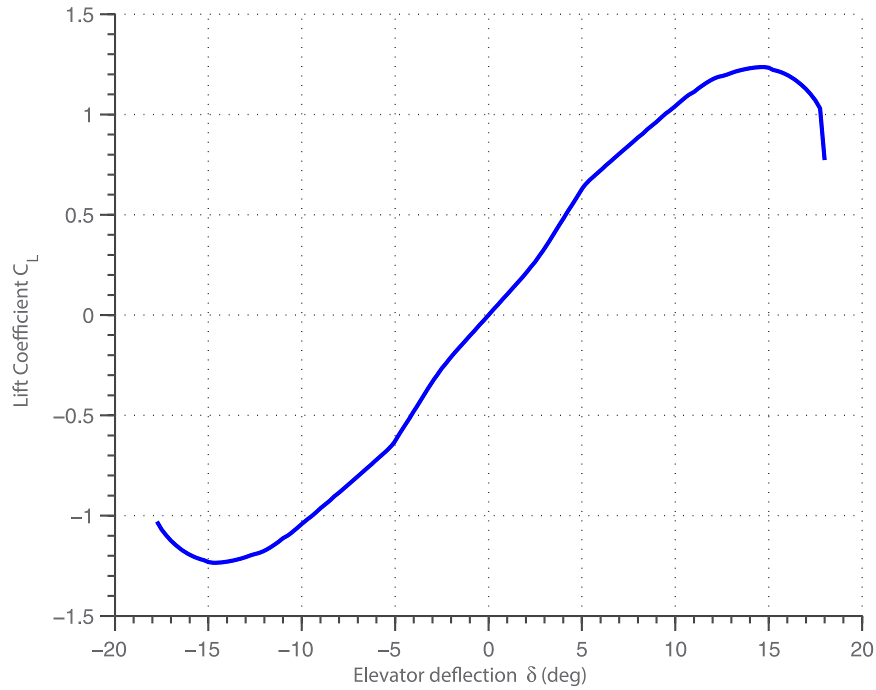

Figure 2. Typical lift coefficient versus fin deflection for the NACA-0012 fin profile at Reynolds number 5×10^5. (Source: Airfoil tool generator at http://airfoiltools.com/airfoil/details?airfoil=n0012-il).

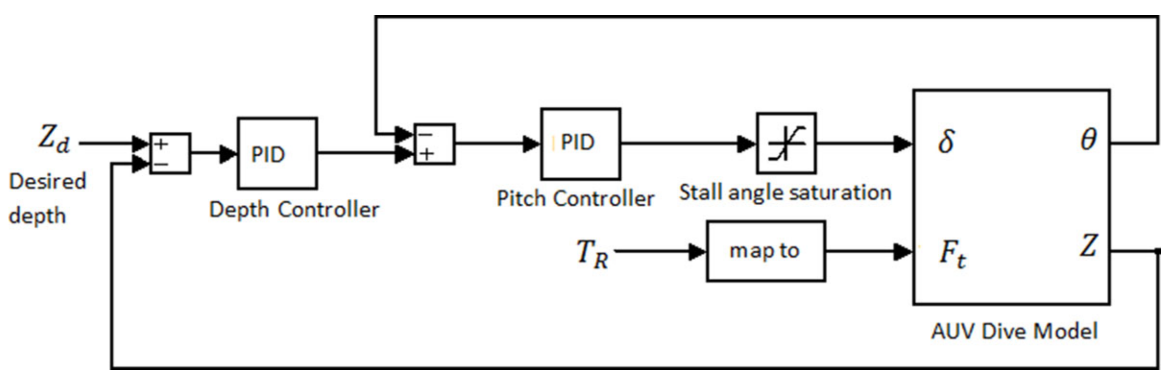

Figure 3. Depth subsystem with dual closed-loop control: inner pitch control and outer depth control.

2.5. Depth Closed-loop System

As illustrated in Figure 3, dual loop control is implemented to regulate the AUV depth. We have pitch control in the inner loop and depth control in the outer loop. The dual-loop implementation is widely used for depth control of the torpedo-shaped AUV (Jalving, 1994; Petrich & Stilwell, 2010; Prestero, 2001). The torpedo-shaped AUV is underactuated, such that the depth and pitch cannot be controlled independently. Hence, given a desired depth, the outer depth control loop is used to generate the desired pitch angle, which is then fed into the inner pitch control loop to generate the elevator command.

Here, the proportional-integral (PI) controllers are employed in both the inner and outer loops. An integral controller is needed in order to remove the steady-state error when a step input is fed. We assume that the depth and pitch controllers will stabilize the plant when the AUV's operating speed is larger than the minimum speed. This is a reasonable assumption, as such controllers should already be functioning in basic AUV operations.

3. MINIMUM SPEED AND ITS CHARACTERISTICS

In this section, we begin with the calculation of the minimum speed based on the model described in Section 2. First,

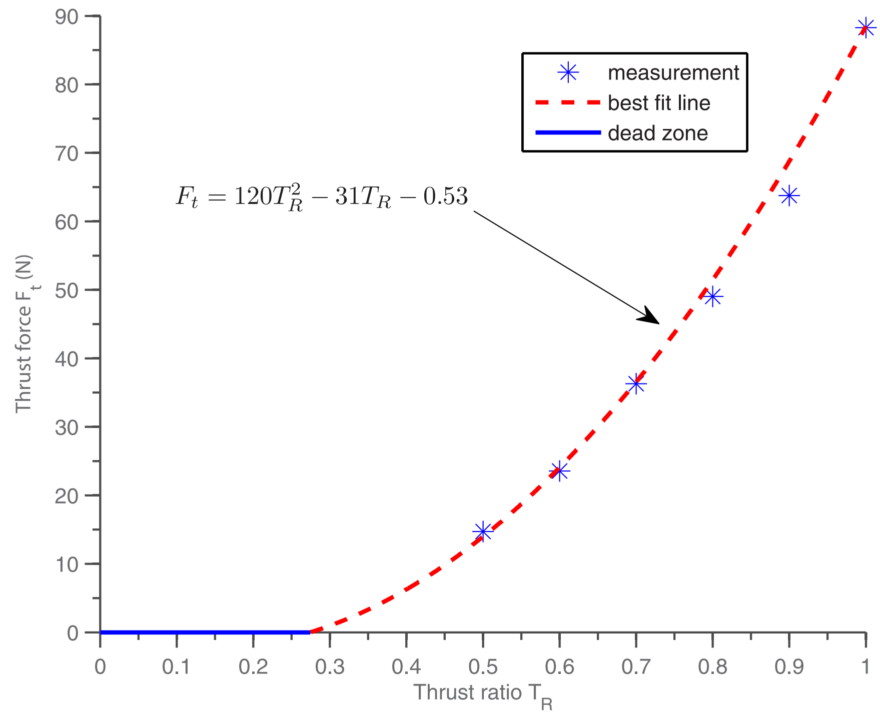

Figure 4. Relationship between thrust ratio T_R and thrust force F_t for the Tecnadyne Model 520 underwater thruster.

the formal definition of the minimum speed is given. Next, we derive the equations for two important curves: maximum required pitch curve and achievable pitch curve. We then argue that the minimum speed occurs at the intersection of these two curves. The final solution of the minimum speed is then derived together with its condition of existence. By analyzing the maximum required pitch curve and the achievable pitch curve, we study how the buoyancy, righting moment, and the fin's effectiveness affect the minimum speed. In Section 3.2, we observe how the *STARFISH* AUV loses its pitch-controllability when it cruises below the minimum speed. There are two strong indications when the AUV loses its pitch-controllability: the pitch response deviates from the desired pitch, and the elevator deflection becomes saturated.

3.1. The Minimum Speed

Let us first define the minimum speed of an AUV. The minimum speed is the vehicle's speed when

1. The depth rate defined by Eq. (1) is equal to zero, $\dot{Z} = 0$.
2. The elevator deflection δ is at its maximum value, $\delta = \delta_{\max}$.
3. The AUV is at an equilibrium point of Eq. (3), $\dot{\mathbf{x}} = 0$.

To maintain depth, the depth rate should be equal to zero. So from Eq. (1), we solve for the relationship between α and θ:

$$\dot{z} = V[-\cos\alpha\sin\theta + \sin\alpha\cos\theta] = 0 \Rightarrow \alpha = \theta, \quad (17)$$

which means that for constant depth maneuver, the angle of attack is equal to the pitch angle.

When the AUV is at equilibrium, we have

$$\mathbf{R}(\mathbf{x}) + \mathbf{F}(\mathbf{x}, \mathbf{u}) = \mathbf{0} \quad (18)$$

because $\mathbf{ET}(\mathbf{x})$ in Eq. (3) is nonsingular for a slender vehicle at nonzero speed, as pointed out by Petrich et al. (2007).

Then, Eq. (18) is expanded to

$$\begin{pmatrix} -m_z qV\sin\alpha - mx_{cg}q^2 \\ m_x qV\cos\alpha + mz_{cg}q^2 \\ (m_z - m_x)V^2\cos\alpha\sin\alpha - m(x_{cg}\cos\alpha + z_{cg}\sin\alpha)qV \\ q \end{pmatrix} = -\begin{pmatrix} F_x(\mathbf{x}, \mathbf{u}) \\ F_z(\mathbf{x}, \mathbf{u}) \\ M_y(\mathbf{x}, \mathbf{u}) \\ 0 \end{pmatrix}. \quad (19)$$

The last row requires the pitch rate to be zero, $q = 0$, and Eq. (19) becomes

$$F_x(\mathbf{x}, \mathbf{u}) = 0, \quad (20)$$

$$F_z(\mathbf{x}, \mathbf{u}) = 0, \quad (21)$$

$$M_y(\mathbf{x}, \mathbf{u}) = -(m_z - m_x)V^2\cos\alpha\sin\alpha. \quad (22)$$

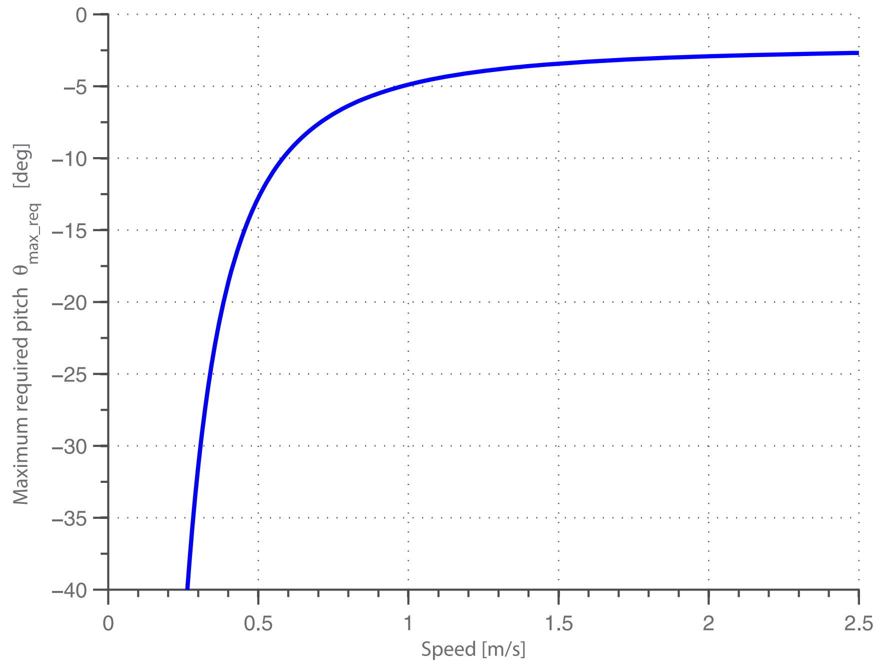

Figure 5. The maximum required pitch curve.

Calculating (20)× $\cos\theta +$ (21)× $\sin\theta$, and knowing $\alpha = \theta$, we have

$$F_D(V, \alpha, \delta) = -F_t \cos\theta, \tag{23}$$

and substituting $F_D(V, \alpha, \delta)$ from Eq. (11), we obtain

$$\frac{1}{2}\rho V^2 A_b C_{D_0} = -F_t \cos\theta. \tag{24}$$

Calculating (20)× $\sin\theta -$ (21)× $\cos\theta$, and knowing $\alpha = \theta$, we have

$$F_L(V, \alpha, \delta) + (F_w - F_B) = F_t \sin\theta, \tag{25}$$

and substituting $F_L(V, \alpha, \delta)$ from Eq. (12), we obtain

$$\frac{1}{2}\rho V^2\{A_b C_{L_\alpha}\alpha + A_f C_{L_\delta}\delta\} + (F_w - F_B) = F_t \sin\theta. \tag{26}$$

By combining Eqs. (24) and (26), and knowing $\alpha = \theta$, $\delta = \delta_{\max}$, and assuming θ to be a small angle ($\sin\theta \approx \theta, \tan\theta \approx \theta$), we solve θ as a function of V as

$$\theta_{\text{max\_req}} = \frac{F_B - F_w}{\frac{1}{2}\rho A_b\left(C_{L_\alpha} + C_{D_0}\right)V^2} - \frac{A_f C_{L_\delta}\delta_{\max}}{A_b\left(C_{L_\alpha} + C_{D_0}\right)}. \tag{27}$$

We denote the pitch angle calculated from Eq. (27) as $\theta_{\text{max\_req}}$ because it is the maximum pitch angle that is required to overcome the positive buoyancy of the AUV during level flight at various speeds. To maintain depth, the vehicle must be pitched nose down enough for the thruster force to counteract both the positive buoyancy of the vehicle and the upward force generated by the control fins. Unfortunately, larger pitch angles require greater control fin deflections, which causes a larger upward force on the vehicle from the control fins. $\theta_{\text{max\_req}}$ is the downward pitch angle that is needed, at a given speed, to counteract both the positive buoyancy of the vehicle and the upward force generated by the control fins at their maximum deflection.

For example, if the AUV is traveling at 1 m/s, Figure 5 indicates that $\theta_{\text{max\_req}} = -5^\circ$. However, in reality, as the minimum speed is not 1 m/s and thus δ is not at its maximum value, the AUV is pitching down at a smaller[2] pitch angle during level flight. So, in this sense, the maximum required pitch curve indicates the largest pitch angle that is required to maintain level flight, which only occurs at the minimum speed.

Next, we calculate the achievable pitch angle θ_{ach} by solving the pitch moment balance in Eq. (22) when the elevator deflection δ is set to its maximum, $\delta_{\max}$. Substituting Eqs. (9) and (13) into Eq. (22), we have

$$\begin{aligned}&\frac{1}{2}\rho V^2\{A_b L[C_{m_\alpha}\alpha + C_{m_q}q] + A_f x_f C_{L_\delta}\delta\}\\ &- (x_{cg}\cos\theta + z_{cg}\sin\theta)F_w\\ &= -(m_z - m_x)V^2\cos\alpha\sin\alpha. \end{aligned}\tag{28}$$

Given $\alpha = \theta$, $q = 0$, $\delta = \delta_{\max}$, and assuming θ to be a small angle and $x_{cg} = 0$, we solve θ_{ach} as a function of V as

$$\theta_{\text{ach}} = \frac{\frac{1}{2}\rho A_f x_f C_{L_\delta}\delta_{\max}V^2}{z_{cg}F_w - \left[\frac{1}{2}\rho A_b L C_{m_\alpha} + (m_z - m_x)\right]V^2}. \tag{29}$$

[2] In terms of magnitude.

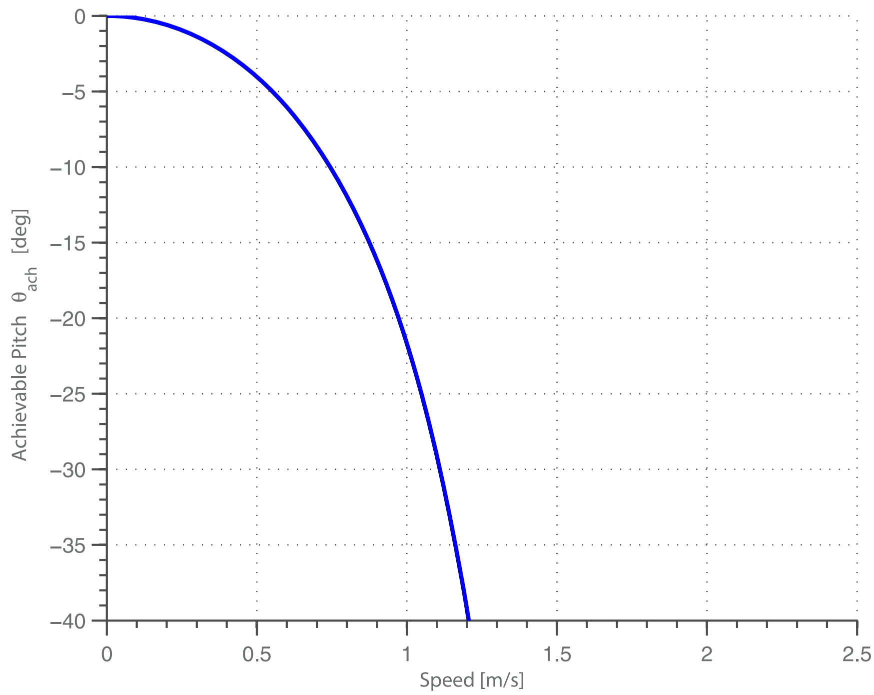

Figure 6. The achievable pitch curve.

We denote the pitch angle calculated from Eq. (29) as θ_{ach} because it is the achievable pitch angle when elevator deflection is commanded to its maximum value. As the vehicle's speed V becomes smaller, the achievable pitch angle becomes smaller, as shown in Figure 6. The achievable pitch angle increases with the vehicle speed due to the Munk moment (Triantafyllou & Hover, 2002, p. 56):

$$M_{\text{Munk}} = (m_z - m_x)V^2 \cos\alpha \sin\alpha. \tag{30}$$

The Munk moment is destabilizing as it acts in the opposite direction of a body restoring moment and a hydrostatic righting moment. At high speed and a large angle of attack, the Munk moment becomes larger than the sum of the body restoring moment and the hydrostatic righting moment.

The minimum speed is found by equating Eqs. (27) and (29). The concept is visualized through Figure 7, where $\theta_{\text{max\_req}}$ and θ_{ach} are plotted against speed. The minimum speed occurs at the intersection of the two curves. It occurs at the largest $\theta_{\text{max\_req}}$ that is achievable.

By equating Eqs. (27) and (29), we obtain

$$\frac{\frac{1}{2}\rho A_f x_f C_{L_\delta} \delta_{\max} V^2}{z_{cg} F_w - \left[\frac{1}{2}\rho A_b L C_{m_\alpha} + (m_z - m_x)\right] V^2} = \frac{F_B - F_w}{\frac{1}{2}\rho A_b \left(C_{L_\alpha} + C_{D_0}\right) V^2} - \frac{A_f C_{L_\delta} \delta_{\max}}{A_b \left(C_{L_\alpha} + C_{D_0}\right)}. \tag{31}$$

Define the following variables:

$$\beta_1 = \frac{1}{2}\rho A_f x_f C_{L_\delta} \delta_{\max}, \tag{32}$$

$$\beta_2 = z_{cg} F_w, \tag{33}$$

$$\beta_3 = \frac{1}{2}\rho A_b L C_{m_\alpha} + (m_z - m_x), \tag{34}$$

$$\beta_4 = F_B - F_w, \tag{35}$$

$$\beta_5 = \frac{1}{2}\rho A_b \left(C_{L_\alpha} + C_{D_0}\right), \tag{36}$$

$$\beta_6 = \frac{A_f C_{L_\delta} \delta_{\max}}{A_b \left(C_{L_\alpha} + C_{D_0}\right)}, \tag{37}$$

and thus simplify Eq. (31) to

$$\frac{\beta_1 V^2}{\beta_2 - \beta_3 V^2} = \frac{\beta_4}{\beta_5 V^2} - \beta_6. \tag{38}$$

Then Eq. (38) is rewritten as a quadratic equation by treating V^2 as a variable:

$$V^4 + \frac{\beta_3\beta_4 + \beta_2\beta_5\beta_6}{\beta_1\beta_5 - \beta_3\beta_5\beta_6} V^2 - \frac{\beta_2\beta_4}{\beta_1\beta_5 - \beta_3\beta_5\beta_6} = 0. \tag{39}$$

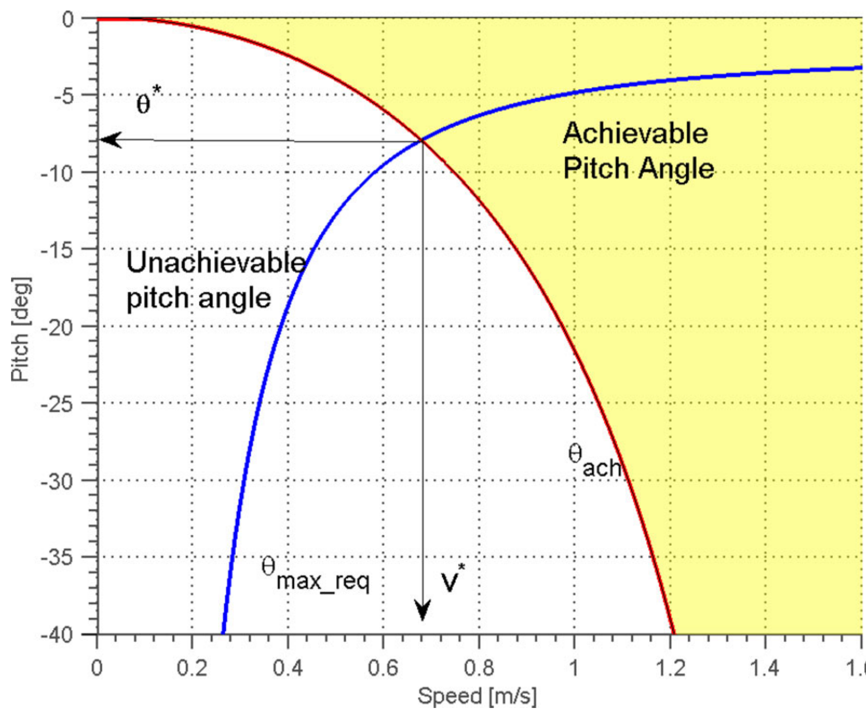

Figure 7. The minimum speed. Minimum speed is found at the intersection of the required pitch curve and the achievable pitch curve.

Since the square of the minimum speed should be a real number, the discriminant of the quadratic equation needs to be greater than or equal to zero,

$$\left(\frac{\beta_3\beta_4+\beta_2\beta_5\beta_6}{\beta_1\beta_5-\beta_3\beta_5\beta_6}\right)^2+4\left(\frac{\beta_2\beta_4}{\beta_1\beta_5-\beta_3\beta_5\beta_6}\right)\geq 0. \tag{40}$$

For a positive buoyant ($F_B > F_w$) AUV with the center of gravity below the center of buoyancy ($z_{cg} > 0$), we have

$$\beta_2\beta_4 = z_{cg}F_w(F_B - F_w) > 0. \tag{41}$$

So, in order to fulfill Eq. (40) and to have a finite minimum speed, we need to satisfy

$$\beta_1\beta_5 - \beta_3\beta_5\beta_6 > 0. \tag{42}$$

As $\beta_5 < 0$,

$$\beta_1 - \beta_3\beta_6 < 0. \tag{43}$$

By substituting the corresponding β_i, Eq. (43) becomes

$$\frac{1}{2}\rho A_f x_f C_{L_\delta}\delta_{\max} - \left[\frac{1}{2}\rho A_b L C_{m_\alpha} + (m_z - m_x)\right] \times \frac{A_f C_{L_\delta}\delta_{\max}}{A_b(C_{L_\alpha}+C_{D_0})} < 0. \tag{44}$$

Given $C_{L_\alpha} < 0$, $C_{D_0} < 0$, and $(m_z > m_x)$ for a slender AUV, we then obtain

$$C_{m_\alpha} > \frac{x_f}{L}\left(C_{L_\alpha}+C_{D_0}\right) - \frac{(m_z-m_x)}{\frac{1}{2}\rho A_b L}. \tag{45}$$

By its definition of the body-restoring moment, we know $C_{m_\alpha} < 0$. Finally, for the existence of minimum speed, it is required that

$$\frac{x_f}{L}\left(C_{L_\alpha}+C_{D_0}\right) - \frac{(m_z-m_x)}{\frac{1}{2}\rho A_b L} < C_{m_\alpha} < 0. \tag{46}$$

Figure 8 illustrates the nonexistence of minimum speed when inequality (46) is not satisfied. The θ_{ach} curve and the $\theta_{\text{max\_req}}$ curve do not intersect one another even when the speed goes to infinity. This is because the restoring moment is too large for the AUV even to pitch down at the required angle to maintain depth.

If the minimum speed exists, it can be calculated by solving the quadratic equation (39), so that

$$V_{\min}^2 = -\left(\frac{\beta_3\beta_4+\beta_2\beta_5\beta_6}{2(\beta_1\beta_5-\beta_3\beta_5\beta_6)}\right) \pm\sqrt{\left(\frac{\beta_3\beta_4+\beta_2\beta_5\beta_6}{2(\beta_1\beta_5-\beta_3\beta_5\beta_6)}\right)^2+\left(\frac{\beta_2\beta_4}{(\beta_1\beta_5-\beta_3\beta_5\beta_6)}\right)}. \tag{47}$$

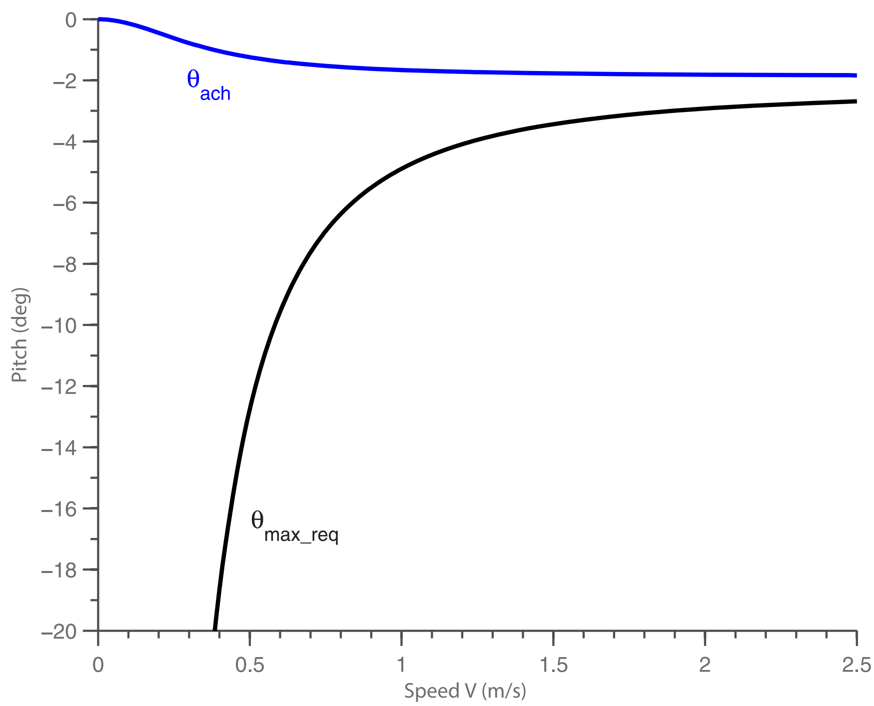

Figure 8. Nonexistence of the minimum speed.

The solution consists of three important group of terms:

$$\beta_3\beta_4 + \beta_2\beta_5\beta_6 = \left(\frac{1}{2}\rho A_b L C_{m_\alpha} + (m_z - m_x)\right)(F_B - F_w) + \frac{1}{2}\rho z_{cg} F_w A_f C_{L_\delta}\delta_{\max}, \tag{48}$$

$$\beta_1\beta_5 - \beta_3\beta_5\beta_6 = \left(\frac{1}{2}\rho A_b(C_{L_\alpha} + C_{D_0})\right)\left(\frac{1}{2}\rho A_f x_f C_{L_\delta}\delta_{\max}\right) - \left(\frac{1}{2}\rho A_b L C_{m_\alpha} + (m_z - m_x)\right)\left(\frac{1}{2}\rho A_f C_{L_\delta}\delta_{\max}\right), \tag{49}$$

$$\beta_2\beta_4 = z_{cg} F_w (F_B - F_w). \tag{50}$$

The corresponding pitch angle at $V_{\min}$ can be calculated by substituting $V_{\min}$ into Eq. (27):

$$\theta^* = \frac{F_B - F_w}{\frac{1}{2}\rho A_b \left(C_{L_\alpha} + C_{D_0}\right) V_{\min}^2} - \frac{A_f C_{L_\delta}\delta_{\max}}{A_b\left(C_{L_\alpha} + C_{D_0}\right)}, \tag{51}$$

and the corresponding thrust force at $V_{\min}$ is given by Eq. (24) as

$$F_t^* = -\frac{1}{2}\rho V_{\min}^2 A_b C_{D_0}\cos\theta^*. \tag{52}$$

The minimum thrust ratio T_R^* is then given by substituting F_t^* into Eq. (16) and solving it:

$$F_t^* = 120(T_R^*)^2 - 31T_R^* - 0.53. \tag{53}$$

The following statements can be deduced from analyzing both the maximum required pitch curve and the achievable pitch curve:

- The minimum speed is proportional to the buoyancy of the AUV. If the AUV is more buoyant, the minimum speed will increase. The buoyancy affects only the $\theta_{\text{max\_req}}$ curve, as shown in Figure 9. The increase in the minimum speed is coupled with the decrease of the pitch angle, θ^*.
- The minimum speed is proportional to the metacentric height, z_{cg}. The greater the metacentric height, the greater is the righting moment and thus the higher is the minimum speed. Metacentric height affects only the θ_{ach} curve, as shown in Figure 10. The increase of minimum speed is coupled with the increase of the pitch angle, θ^*.
- The minimum speed is *inversely* proportional to the fin's effectiveness, $x_f A_f C_{L_\delta}$. The larger x_f, A_f, and C_{L_δ} are, the more the minimum speed will be reduced. The fin's effectiveness affects both the $\theta_{\text{max\_req}}$ curve and θ_{ach}, as shown in Figure 11. The reduction in the minimum speed is coupled with the decrease of the pitch angle, θ^*.
- It is also noticed that the minimum speed is independent of the viscous drag coefficient (M_q) and the moment of inertia (J_y).

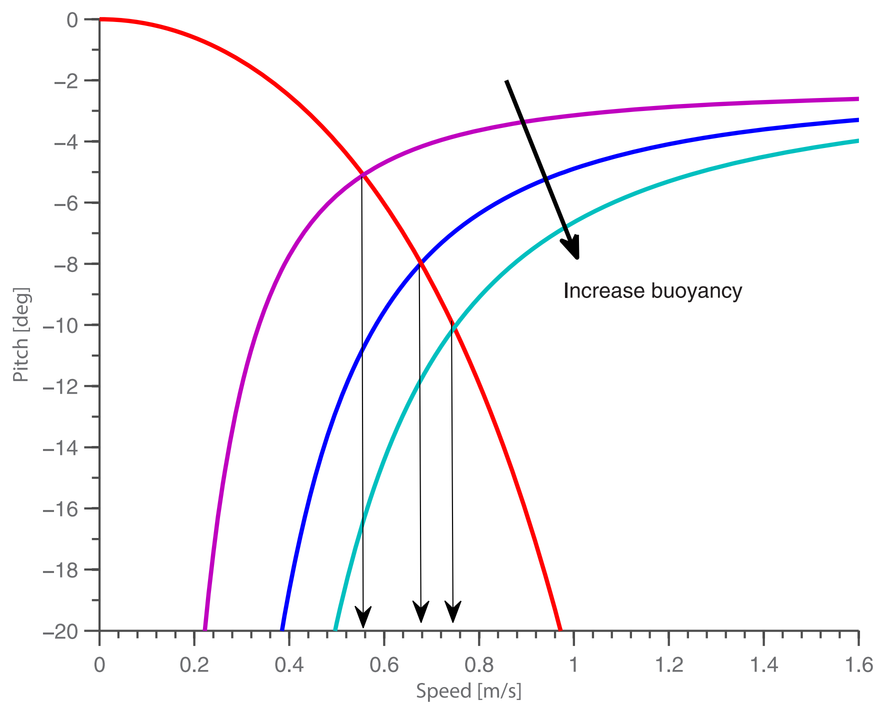

Figure 9. Effect of buoyancy on minimum speed.

In practice, one could reduce the minimum speed of an AUV by reducing the buoyancy, and the metacentric height, or by increasing the fin's effectiveness. From the analysis, manipulating the buoyancy is a better option because the reduction of the minimum speed by means of buoyancy is coupled with the smaller pitch down angle. On the contrary, reduction of minimum speed by means of metacentric height or the fin's effectiveness is coupled with a bigger pitch down angle, which is undesirable due to a larger drag.

In reality, there are physical constraints on how much one can manipulate buoyancy, metacentric height, and the fin's effectiveness. For example, buoyancy cannot be reduced to zero, as the AUV needs to float to the surface for easy recovery under power failure or other emergency conditions. The metacentric height is needed to make sure that the AUV is always upright, and to keep the roll of the AUV small. It should be noted that when one factor is changed, the rest of the factors might be affected simultaneously. For instance, changing the buoyancy of the AUV by adding weight might affect the metacentric height concurrently.

3.2. Characteristic of Losing Pitch-Controllability

An experiment was conducted to investigate the phenomenon of losing pitch-controllability when the AUV's speed drops below its minimum speed. There were three stages in this experiment (see Figure 12):

- Stage 1 ($0 \leq t < 12$ s): The AUV was driven at a speed of $u_0 = 1.4$ m/s until it reached a depth of 2 m.
- Stage 2 ($12 \leq t < 40$ s): The speed was reduced gradually up to a point just before the AUV lost its pitch-controllability.
- Stage 3 ($t \geq 40$ s): The speed was reduced beyond its minimum speed, causing the AUV to lose its pitch-controllability.

Consider the transition between Stage 2 and Stage 3. From the pitch response in Stage 2, it is observed that the pitch response followed the desired pitch angle θ_d closely and the pitch error[3] θ_e was close to zero. In Stage 3, the pitch error grew significantly, indicating the loss of pitch-controllability as the pitch response deviated from the desired pitch. In the elevator plot from Stage 2 to Stage 3, it is observed that the elevator was becoming saturated at its maximum value. In the depth response plot, it is observed that the AUV was losing depth gradually, but its effect was

[3]Pitch error $\theta_e \doteq \theta - \theta_d$.

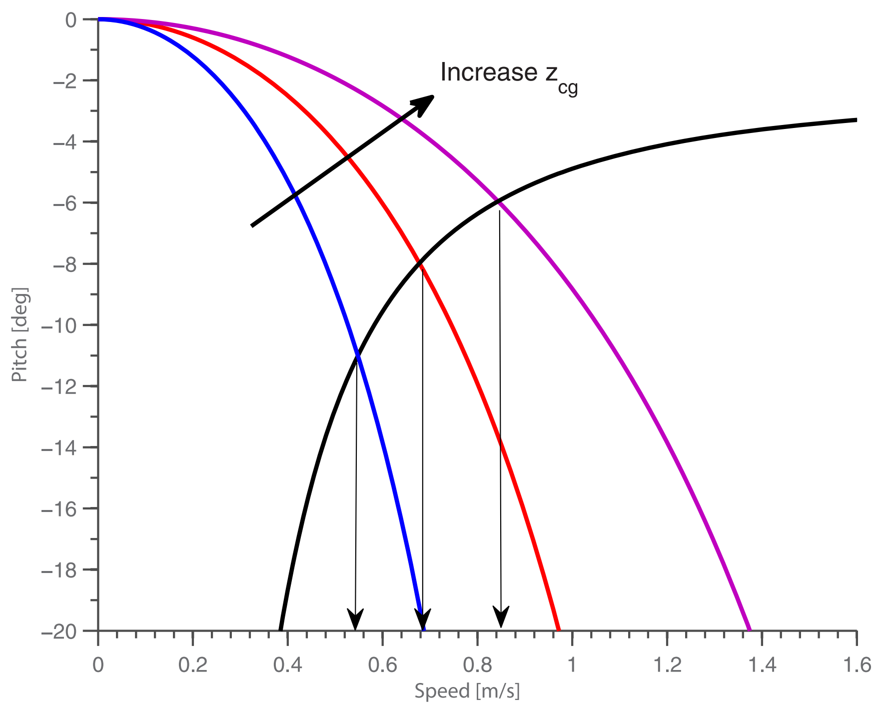

Figure 10. Effect of metacentric height on minimum speed.

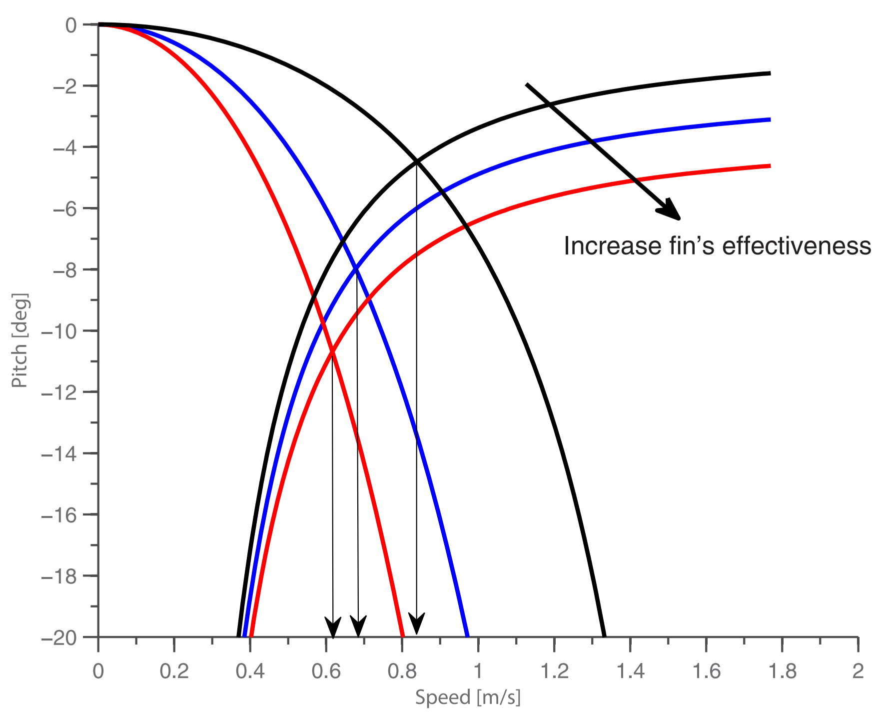

Figure 11. Effect of the fin's effectiveness on the minimum speed.

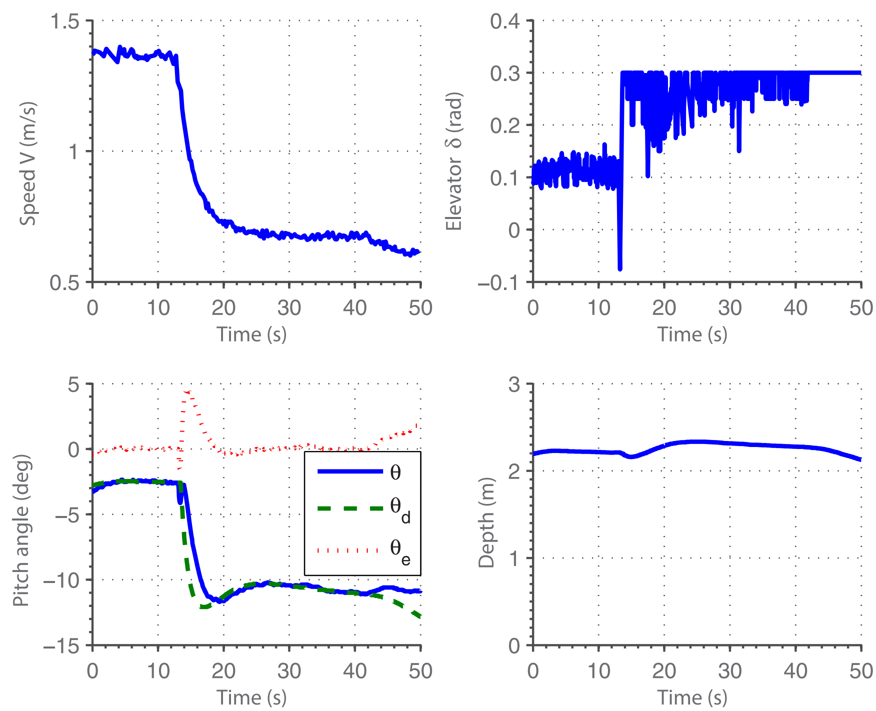

Figure 12. Characteristic of losing pitch-controllability. From 40 s onward, the pitch response deviated from the desired pitch and the elevator became saturated.

not as fast and significant as seen in the pitch response plot. In summary, it is observed that when the AUV was losing its pitch-controllability, the pitch response deviated from the desired pitch and the elevator became saturated.

4. MINIMUM SPEED SEEKING ALGORITHM

In this section, we discuss the minimum speed seeking algorithm under the framework of extremum seeking (ES) (Tan, Moase, Manzie, Nesic, & Mareels, 2010). There is difficulty in applying the existing methods in ES to solve the minimum speed problem. The problem violates important assumptions that the steady-state characteristics of the plant will be well defined and stable, regardless of the input parameter. We relax these assumptions by introducing a new definition of steady-state mapping that imposes a new structure on the seeking algorithm. This leads naturally to a detailed discussion on the proposed seeking algorithm in Section 4.2.

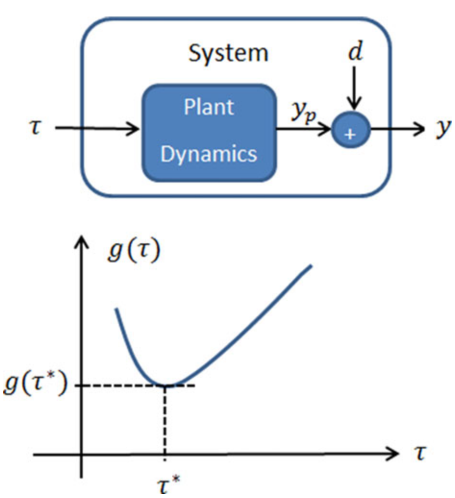

Figure 13. Input-output system with a steady-state map.

4.1. Extremum Seeking

The minimum speed seeking problem could be studied under the framework of ES. Typically, ES is employed to find the optimal operating condition for industrial processes to produce better outcomes, productivity, or yield. The optimal operating condition is not known analytically, or it might change with time. Hence, optimization has to be performed online to search for the optimal point by making use of real-time measurement of the actual process (Zhang & Ordâoänez, 2012).

We describe a typical extremum seeking problem using a single-input single-output system, as shown in Figure 13. The dynamic plant has a real value input parameter, denoted by $\tau \in \Re$. For any fixed τ, the system converges to a steady state uniquely determined by τ. In other words, under a fixed input, the cost output $y_p = h(x)$, as a function of system state x, converges to a constant value. In this case, a function $g : \Re \rightarrow \Re$, given as a limit

$$g(\tau) := \lim_{t\to\infty} y_p(t)\Big|_{\text{input fixed at } \tau,} \tag{54}$$

is well defined, and this function $g(\cdot)$ is called a *readout* map (Teel & Popovic, 2001). The goal of extremum seeking is to drive the input/output pair from the initial $[\tau_0, g(\tau_0)]$ to the optimal $[\tau^*, g(\tau^*)]$ given measurements of input τ and output $y = y_p + d$, where d is a bounded disturbance.

Starting from some initial values, the ES algorithm modifies the input parameter, monitors the plant's response to obtain the gradient of $g(\tau)$, and then adjusts the parameter toward the optimal point. The most popular scheme of ES is the method of sinusoidal perturbation where the input parameter is perturbed and updated continuously. Alternatively, the input parameter could be updated in a discrete manner. A step change is made on the parameter, and then the algorithm takes some time to measure the steady-state response before another step change. The stability proof of the first and second methods is given in Krstić and Wang (2000) and Teel & Popovic (2001), respectively.

Unfortunately, the stability analysis requires the system to be locally exponentially stable for every point in the *readout* map. Specifically, the input parameter in our study is the AUV thrust, and there exists a range of thrusts[4] that will cause the AUV to lose controllability and become unstable. Define

$$y_p = T_R + k\theta_e, \tag{55}$$

where k is a positive constant and the negative value of pitch error θ_e is truncated to zero so that $\theta_e \geq 0$. Then

$$g(T_R) := \lim_{t\to\infty} [T_R(t) + k\theta_e(t)]\Big|_{\text{input fixed at } T_R} \tag{56}$$

will result in a *readout* map as shown in Figure 14. This is because

$$\lim_{t\to\infty} \theta_e(t)\Big|_{\text{input fixed at } T_R<T_R^*} = +\infty \tag{57}$$

and

$$\lim_{t\to\infty} \theta_e(t)\Big|_{\text{input fixed at } T_R\geq T_R^*} \approx 0. \tag{58}$$

The *readout* map in Figure 14 is not well defined and is unstable for inputs less than T_R^*. Since the required assumptions are violated, the stability of existing ES methods is not guaranteed. However, a change in the definition of $g(\cdot)$ could result in a well-defined and stable *readout* map.

[4]All values of thrust that have corresponding speeds less than the minimum speed.

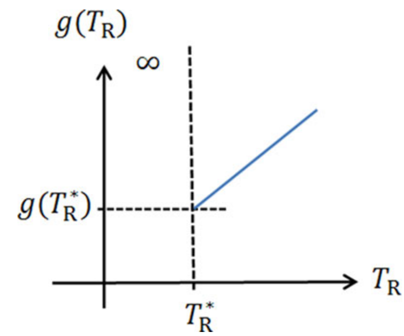

Figure 14. Readout map for $g(T_R)$. The *readout* map is not well defined for inputs less than T_R^*.

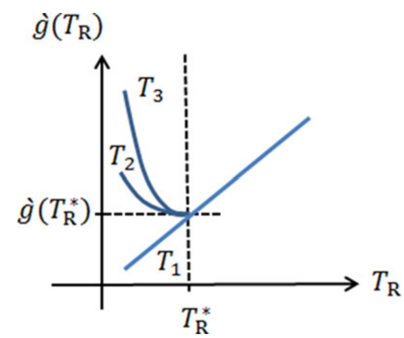

Figure 15. Readout map for $\breve{g}(T_R)$. A change in the definition of $g(\cdot)$ results in a well-defined *readout* map.

Instead of letting time go to infinity, define $g(\cdot)$ by having the time approach a finite value T, where $0 < T < \infty$. To uniquely determine the value of such a definition, the value of the input parameter at time $t = 0$ needs to be fixed. We choose that value to be T_R^*. Therefore, we have

$$\breve{g}(T_R) := \lim_{t\to T} [T_R(t) + k\theta_e(t)]\Big|_{\text{input fixed at } T_R,\text{ and at } t=0, T_R=T_R^*}. \tag{59}$$

Figure 15 shows the plot of $\breve{g}(\cdot)$ for $T = T_1, T_2$, and T_3, where $T_1 < T_2 < T_3$. At time $t = 0$, T_R is equal to T_R^* and thus the pitch error $\theta_e(0) \approx 0$. For the case of $T = T_1 \rightarrow 0^+$, there is no time for the pitch error to grow even though $T_R < T_R^*$. Hence $\breve{g}(T_R) = T_R$. The larger the value of T, the more time there is for the pitch error to grow, and if $T \rightarrow \infty$, then $\breve{g}(T_R)$ is equivalent to the original definition of $g(T_R)$. In summary, we are able to construct a well-defined and stable *readout* map by selecting a proper value of T.

The definition of $\breve{g}(T_R)$ requires $T_R = T_R^*$ at $t = 0$, but the value of T_R^* is not known. This requirement can, however, be fulfilled by performing the following steps. First, discretize the solution space of T_R into a finite number of possible points separated by a constant step size, Δ_T. If the step size is small enough, it is reasonable to assume that T_R^*

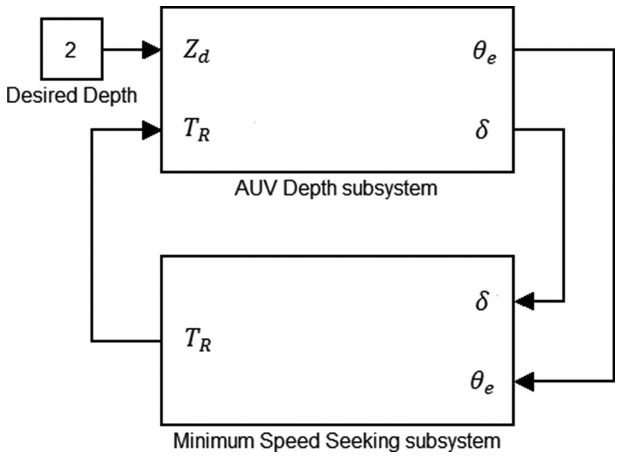

Figure 16. Problem formulation. The block diagram shows the interaction between the AUV depth subsystem and the minimum speed seeking subsystem. The minimum speed seeking subsystem sends a thrust command to the AUV depth subsystem and receives a pitch error θ_e and an elevator deflection δ_s in return.

is equal to a particular point. Then start the search from an initial $T_R(0)$, where $T_R(0) > T_R^*$, and make Δ_T change to T_R at every iteration. Each iteration is time-separated by a seeking period T. Such a seeking method will ensure that $T_R = T_R^*$ before entering the region of $T_R < T_R^*$. Hence, by restricting the search to a small step at every interval of properly selected T, the unstable map (Figure 14) can be transformed to a stable one (Figure 15).

Before describing the seeking algorithm in Section 4.2, the problem is first posed formally. The task of the minimum speed seeking algorithm is as follows: given a real-time measurement of pitch error θ_e and elevator δ_s, force the solution of the closed-loop AUV depth subsystem (Figure 3) to eventually converge to the optimal states where $V = V_{\min}$ from Eq. (47) and $\theta = \theta^*$ from Eq. (51) by manipulating the thrust ratio T_R, and to do so without any precise knowledge of the AUV depth subsystem and the optimal states.

The algorithm resides in the minimum speed seeking subsystem, which augments the AUV depth subsystem by changing the thrust ratio, such that the AUV cruises as slowly as possible while maintaining the desired depth (see Figure 16). It is assumed that when the minimum speed seeking algorithm is turned on, the AUV depth subsystem has already reached steady state at the desired depth and is cruising at a certain speed larger than the minimum speed.

4.2. Seeking Algorithm

Figure 17 illustrates how the seeking algorithm determines the output T_R based on two inputs θ_e and δ_s. A fuzzy inference system (FIS) is used to map the two inputs to three decisions: to keep the current T_R, or to increase or decrease the current T_R by a constant step gain Δ_T. Mathematically, the algorithm can be described as follows:

At every seeking interval k (each interval is separated by seeking period T_S), the thrust ratio is determined by

$$T_R(k) = T_R(k-1) + \Delta T_R, \quad k = 1, 2, 3, \ldots, \tag{60}$$

where

$$\Delta T_R = \begin{cases} -\Delta_T & \text{if FIS output} = -1, \\ 0 & \text{if FIS output} = 0, \\ +\Delta_T & \text{if FIS output} = +1. \end{cases} \tag{61}$$

The seeking algorithm starts to search from an initial thrust ratio $T_R(0)$, a nominal thrust ratio at which the AUV normally operates. It is obvious that $T_R(0)$ is greater than T_R^*.

The period of the seeking loop, denoted by T_S, determines how frequent T_R is changed. The searching algorithm should run at a much slower rate in order to achieve time-scale separation between the nonlinear system dynamics and the seeking loop. This is because the seeking algorithm assumes that the dynamic system functions as a static map, which can be justified only if the time between the change in input parameter is sufficiently long compared to the dynamics of the system. However, T_s also cannot be too large. The seeking algorithm should react fast enough to bring T_R out of the unstable region ($T_R < T_R^*$), or else θ_e may grow unbounded.

From Eq. (60), the algorithm generates a new thrust ratio $T_R(k)$ recursively by adding Δ_T, 0, or $-\Delta_T$ to the previous thrust ratio $T_R(k-1)$. In other words, the thrust ratio is restricted by the maximum change of Δ_T per iteration. As the algorithm drives a dynamical system, a large step will cause a large transient, which is undesirable. By having a known constant step change of thrust ratio Δ_T, there is better control over the time taken for the transient to fade. Furthermore, Δ_T will determine the resolution of the solution by dividing the whole solution space with a step size of Δ_T.

4.2.1. Fuzzy inference system

The fuzzy inference system is chosen because it is a universal mapping tool that allows incorporation of the expert's knowledge via its *if-then* rules. In this study, the FIS is designed as a switching control system where it only yields three crisp output levels for all input values. This is done by using the *Mamdani-type* fuzzy inference system with the largest of maximum (LOM) defuzzification method. The design of such a switching control system using fuzzy set theory is discussed in Perumal and Nagi (2012).

In this section, we discuss mainly how to determine a set of fuzzy rules, and how to design the input and output membership functions and the resulting input-output mapping. For more information on FIS, one could refer to R. Benjamin Knapp (2004).

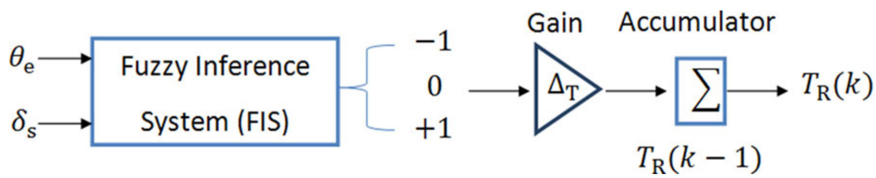

Figure 17. Block diagram of seeking loop. The fuzzy inference system determines whether to maintain, decrease, or increase T_R by a constant step gain Δ_T based on two inputs, θ_e and δ_s, at every seeking interval.

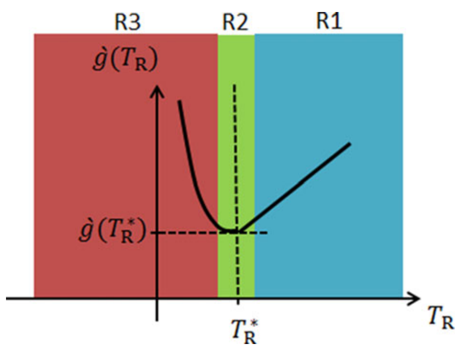

Figure 18. Fuzzy rules and the *readout* map.

As discussed in Section 3.2, when the AUV travels below its minimum speed, the pitch response deviates from the desired pitch and the elevator becomes saturated. Therefore, as long as the elevator is not saturated, T_R could be decreased. When the elevator is saturated and the pitch error is small, it is desirable to keep the current T_R. However, when the elevator is saturated and the pitch error is big, T_R should be increased. The above knowledge is translated to the following fuzzy rules:

1. If (δ is *NotSaturated*), then (Δ_T is *decreased*).
2. If (θ_e is *Small*) and (δ_s is *Saturated*), then (Δ_T is *kept*).
3. If (θ_e is *Big*) and (δ_s is *Saturated*), then (Δ_T is *increased*).

Figure 18 illustrates the active region of each fuzzy rule in the *readout* map. When $T_R \gg T_R^*$, this belongs to the *blue* region and δ_s is far from saturation. Hence, *rule 1* is active and T_R is decreased. When $T_R < T_R^*$, this belongs to the *red* region and δ_s should become saturated, and θ_e starts to grow significantly. Then *rule 3* is activated and T_R is increased. Apparently, *rule 1* and *rule 3* together will force T_R into the *green* region, where *rule 2* is active and T_R is kept unchanged. In practice, T_R^* is changing with time when the AUV is subjected to the disturbance. The cost-driven algorithm will try to track T_R^* by changing T_R continuously and causing T_R to oscillate. In contrast, the proposed algorithm will operate the AUV at a constant T_R that is slightly larger than T_R^*, which is a more desirable behavior.

If we know only the fin saturation without the knowledge of pitch error, we can construct two rules: decrease the T_R when the fin is not saturated, and increase the T_R when the fin is saturated. This will cause the green region R2 to disappear from Figure 18. In this circumstance, the T_R is never kept at a constant value, but it will oscillate around the T_R^* and form a limit cycle, which will affect the controller performance of the AUV. On the other hand, one could keep the T_R constant when the fin is saturated, instead of increase the T_R. In this construction, the seeking algorithm will lost its ability to increase T_R when conditions are not favorable, such as when the AUV encounters a larger disturbance or there is an increase of buoyancy. These are the reasons why the knowledge of pitch error is useful in the algorithm.

Next, all the linguistic terms that are used in the rules need to be defined via membership functions. Two fuzzy sets are used for each input, as shown in Figure 19. The membership functions of pitch error are characterized by the pitch error threshold θ_e^{TS}, which determines the intersection of the two fuzzy sets. For $\theta_e < \theta_e^{TS}$, the error is considered relatively *Small* and acceptable; otherwise, it is considered *Big*. Note that θ_e is considered small when it is negative. The AUV speed needs to be increased when more downward pitching is required (when θ_e is positive). With the increase of speed, the elevator will gain more control authority to close the pitch error gap. On the other hand, when the AUV is pitching down too much (θ_e is negative), there is no need to increase the speed, as the gap can be closed by reducing the elevator deflection. The pitch error threshold θ_e^{TS} is obtained by examining the usual bound of the pitch error during normal AUV maneuvers. One example is given in Figure 20 showing the pitch error changing within a range of 0.01 rad.

Based on the second input δ_s, it is of interest to know how close the elevator is to saturation. The intersection between *Saturated* sets and *NotSaturated* sets is determined by subtracting the elevator fin budget, δ_{FB}, from the maximum elevator angle, δ_{max}. The fin budget δ_{FB} is allocated such that there is enough control authority for the elevator to overcome the environmental disturbance and to keep the pitch at the desired pitch angle. One can select δ_{FB} based on past experiments by looking at the range of the elevator within which the depth is maintained. One example is given in Figure 20 showing the elevator changing within a range of 0.05 rad.

The output consists of three fuzzy sets: *decreased*, *kept*, and *increased* corresponding to values −1, 0, and 1,

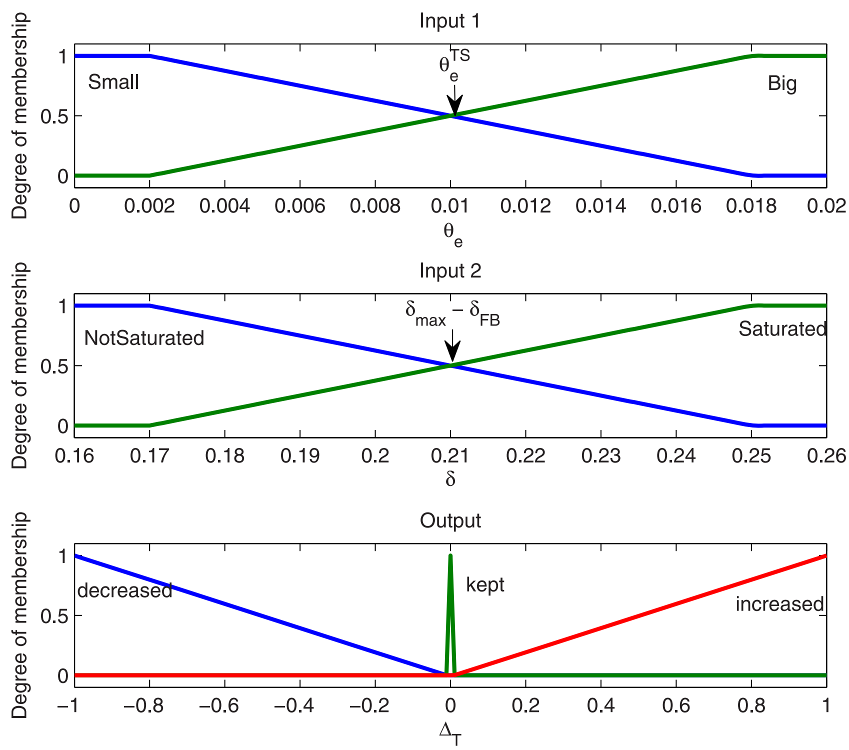

Figure 19. Membership functions of the two inputs and one output. The membership functions of the two inputs, θ_e and δ, are characterized by θ_e^{TS} and δ_{FB}, respectively.

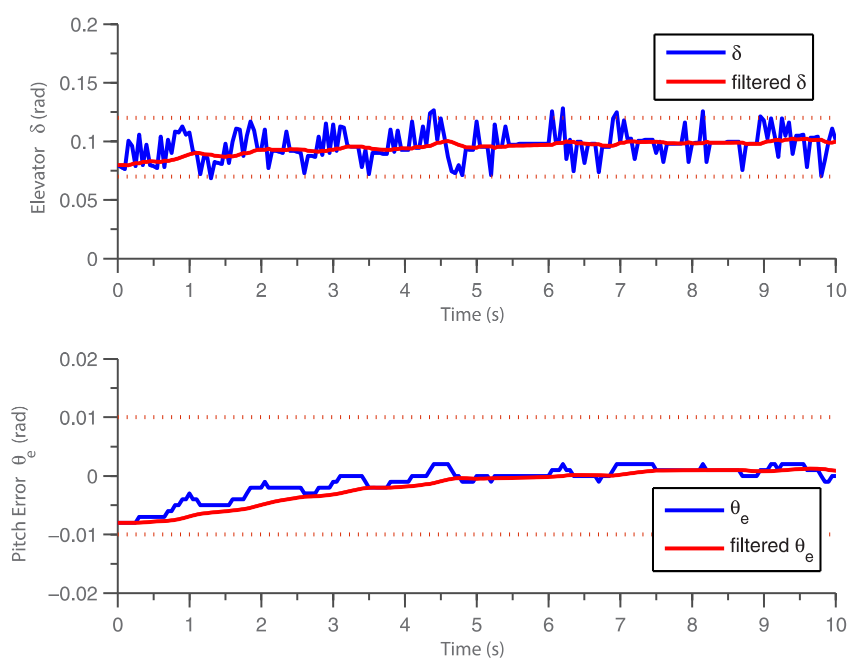

Figure 20. A snapshot of the steady-state elevator and pitch error when the AUV is operating under nominal thrust. This figure is the zoom-in of the first 10 s of Figure 12. The top figure shows the elevator operating within the range of 0.07–0.12 rad, which leads to the assignment of $\delta_{FB} = 0.05$ rad. The bottom graph shows the corresponding pitch error, which leads to the assignment of $\theta_e^{TS} = 0.01$ rad. The figure also shows how the filter smooths θ_e and removes the spikes in δ_s.

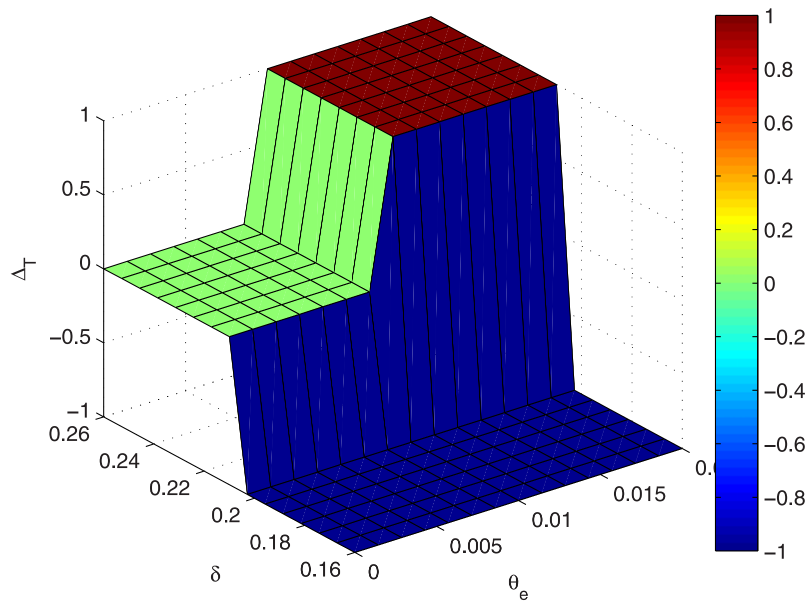

Figure 21. Output surface map of the fuzzy inference system. The plot displays the dependency of the output Δ_T on the two inputs: pitch error θ_e and elevator deflection δ.

respectively, as shown in Figure 19. The design of such an output membership function together with the LOM defuzzification method restricts the output value to three levels similar to a bang-off-bang controller output. This is best illustrated by the output surface map (Figure 21). The output surface has only three distinct colors: red for 1, green for 0, and blue for −1. The output surface map shows that the seeking algorithm will reduce T_R whenever δ_s is not saturated and θ_e is small (blue region). Reduction in T_R will cause δ_s to become saturated eventually. If δ_s is saturated and θ_e is small (green region), T_R will be kept. If the AUV experiences a disturbance that is larger than expected, θ_e will become large. The current T_R is not sufficient to overcome the disturbance and thus T_R needs to be increased (red region). When the disturbance fades away, the vehicle goes back to the blue region. Then the seeking algorithm will reduce T_R until the green region is reached again.

4.2.2. Filtering

Both elevator δ_s and pitch error θ_e are filtered using a low-pass filter (Smith, 1997) of the following form:

$$y(n) = (1 - r)x(n) + ry(n - 1), \quad 0 < r < 1,$$
$$r = \exp(-1/d), \tag{62}$$

where y is the filtered output, x is the input, and d is the filter time constant. In the actual implementation, filtering is performed in the AUV depth subsystem, which runs at 20 Hz, before the data are fed into the minimum speed seeking subsystem. r is chosen as 0.95, which corresponds to $d \approx 20$ samples, equivalent to $T_S = 1$ s. As shown in Figure 20, the signals are filtered to average out the measurement noise and to remove spikes.

5. SIMULATION RESULTS

A simulation model was built in a Matlab/Simulink environment based on the AUV depth subsystem described in Section 2, and the minimum speed seeking subsystem described in Section 4. The two main objectives of performing the simulation are as follows:

- The theoretical minimum speed is known in simulation. It is of interest to find out via simulation how close the seeking algorithm approaches the minimum speed.
- Simulation allows different sets of design parameters to be tested rapidly. Thus we could study the impact of individual design parameter on the seeking performance.

All relevant parameters used in the simulation are listed in Table I.

Figure 22 shows the trajectory of the simulated thrust and speed with respect to time. Initially, the AUV is commanded to thrust at 0.70 until 100 s, which is when the seeking algorithm is turned on. The thrust ratio is reduced to 0.44, which is very close to the optimal thrust ratio ($T_R^* = 0.433$). Despite a small fluctuation seen in the transition stage, the thrust ratio settles down in 50 s. A similar response is seen in the speed, where it settles down to 0.69 m/s, just above the minimum speed ($V_{\min} = 0.678$ m/s).

Figure 23 illustrates how the output of the FIS is driven by the two inputs, δ_s and θ_e. Initially, since δ_s is not

Table I. Simulation parameters.

Design Parameters	Value	Units	Initial Parameters	Value	Units	Controller Parameters	Value	Units
θ_e^{Ts}	0.01	rad	$T_{\mathrm{R}}(0)$	0.7		K_{pz}	−0.15	rad/m
δ_{FB}	0.05	rad	Z_0	2	m	K_{iz}	−0.01	rad/m
T_{S}	1	s	θ_0,α_0,q_0	0	rad, rad/s	$K_{p\theta}$	−20	
Δ_{T}	0.01		V_0	1.4	m/s	$K_{i\theta}$	−0.1	
Model Parameters	**Value**	**Units**	**Model Parameters**	**Value**	**Units**	**Hydrodynamic Parameters**	**Value**	**Units**
ρ	1,000	kg m^{-3}	J_y	40	kg m^2	C_{D_0}	−1.2	
m	66	kg	z_{cg}	0.01	m	C_{L_α}	−1.5	
m_x	70.2	kg	x_{cg}	0	m	C_{L_δ}	−0.3	
m_z	128.8	kg	A_b	0.0314	m^2	C_{M_α}	−1.8	
F_w	647.5	N	A_f	0.0431	m^2	C_{M_q}	−0.8	
F_B	649.4	N	L	2	m	$\delta_{\max}$	0.26	rad
g	9.81	ms^{-2}	x_f	1	m			

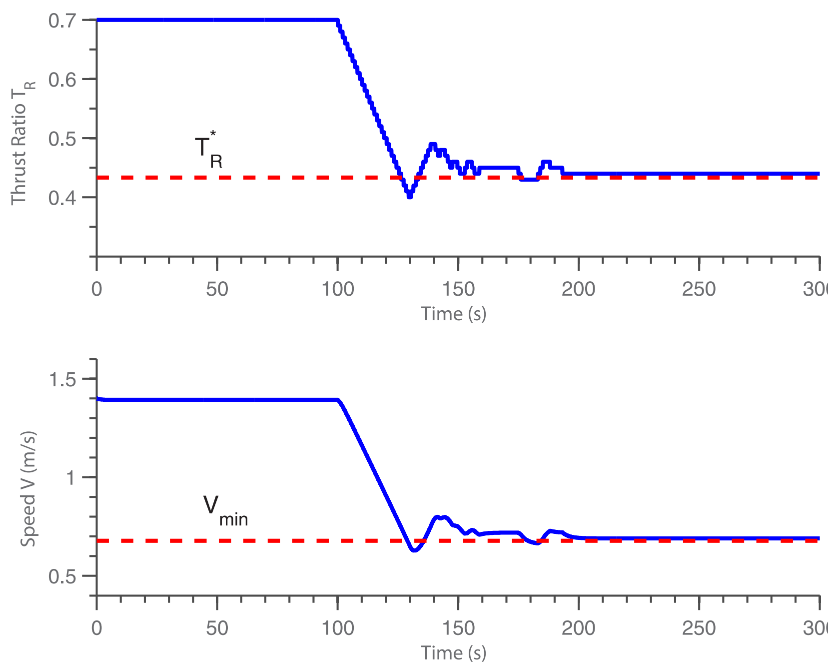

Figure 22. Simulated thrust ratio and speed.

saturated, T_{R} is reduced. To maintain its depth, the AUV needs more downward pitching when the speed is reduced consecutively from 100 to 130 s. θ_{d} decreases faster than θ, causing θ_{e} to grow. At the interval 131–139 s, T_{R} is increased for nine consecutive steps. Then, θ_{e} becomes smaller as the pitch response manages to catch up with the desired pitch. T_{R} is reduced from 0.49 back to 0.44 and stabilizes after 50 s from the start of the seeking algorithm.

As shown in Figure 24, to maintain its depth, the AUV needs to pitch at -1.4° when cruising at 1.4 m/s. While the speed is reduced, the pitch angle decreases and settles down to -7.8°. There is a small oscillation in pitch seen in the transition stage, but in general the pitch response follows the desired pitch closely. The depth is kept at the desired value of 2 m throughout the entire period despite small oscillations during the transition stage.

The minimum speed that can be attained by the seeking algorithm depends on the allocated fin budget δ_{FB} (see Figure 25). The smaller the fin budget, the closer the attainable minimum speed approaches the minimum speed $V_{\min}$, but this is achieved at the expense of robustness against disturbance. In practice, the disturbance always exists; if there is not enough fin budget to overcome the disturbance, fuzzy *rule 3* will be triggered periodically, causing T_{R} to oscillate.

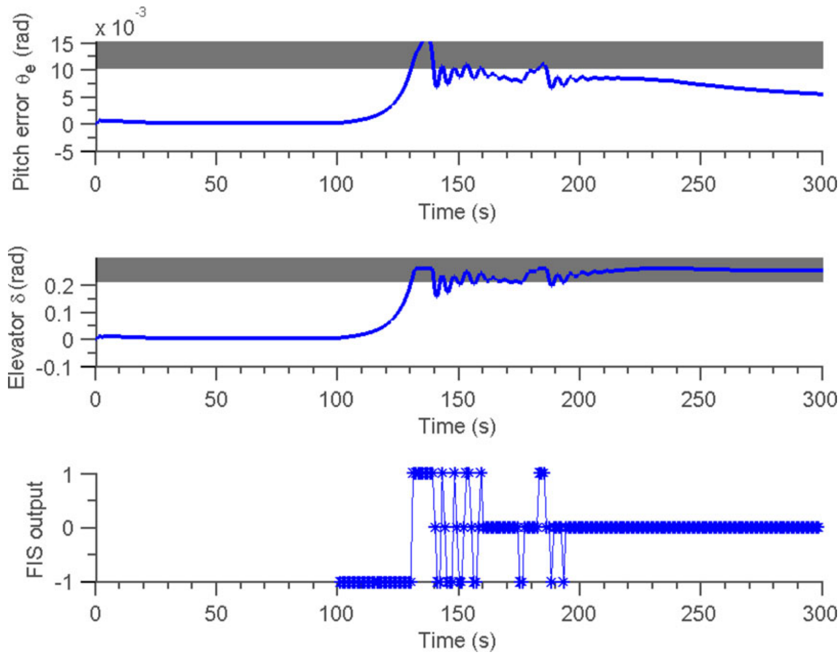

Figure 23. Simulated elevator and pitch error and the corresponding FIS output.

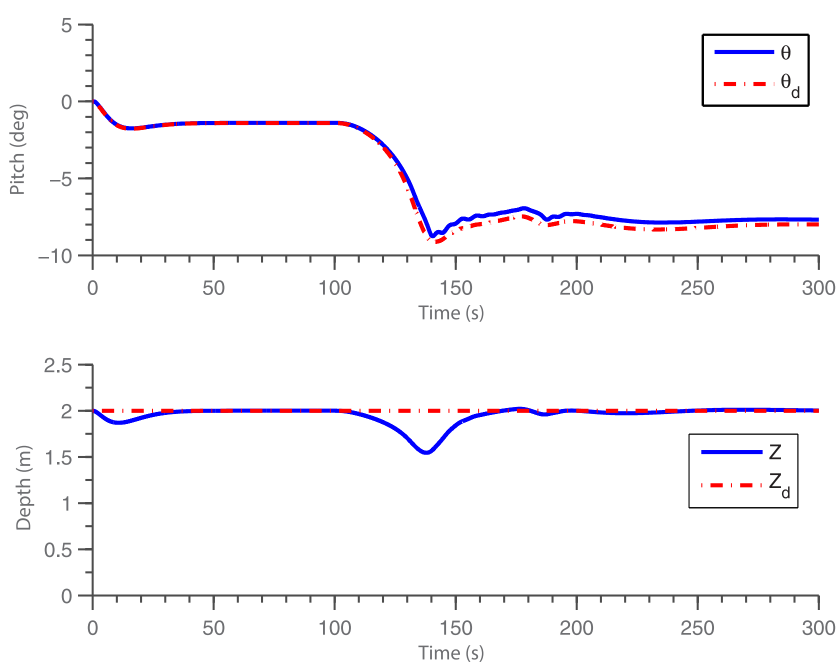

Figure 24. Simulated pitch and depth responses.

Hence, the selection of the fin budget is a tradeoff between optimality and robustness.

Figure 26 shows the convergence of thrust ratio corresponding to different seeking periods T_S. The seeking period determines how frequent the seeking algorithm is executed. To achieve time-scale separation between the pitch dynamics and the seeking dynamics, T_S has to be many times larger than the time constant of pitch dynamics. The simulation results show that the seeking algorithm is unstable for $T_S = 0.5$ s, which causes bounded oscillation of

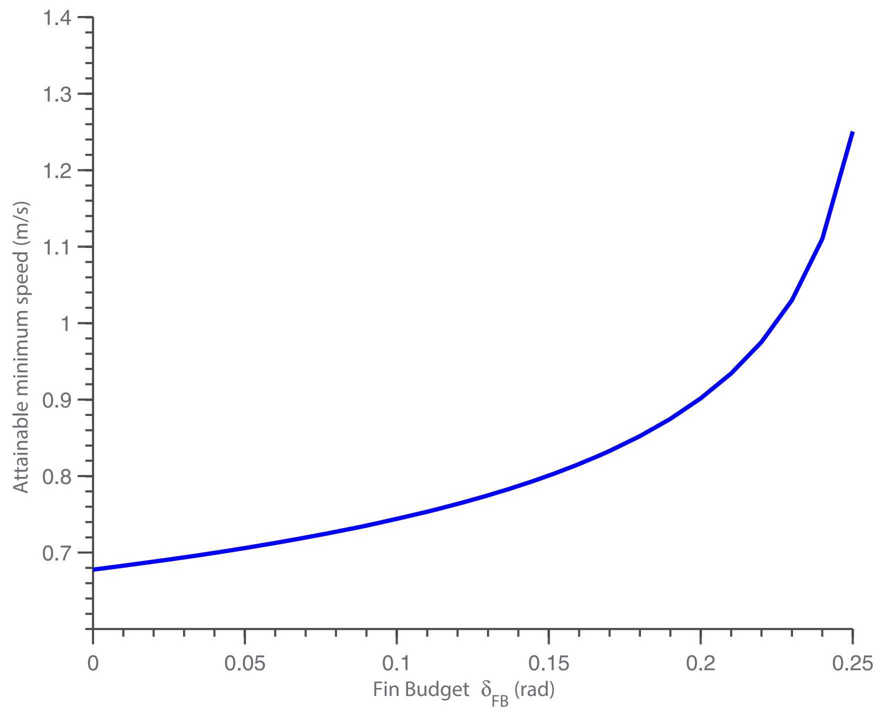

Figure 25. Attainable minimum speed versus allocated fin budget.

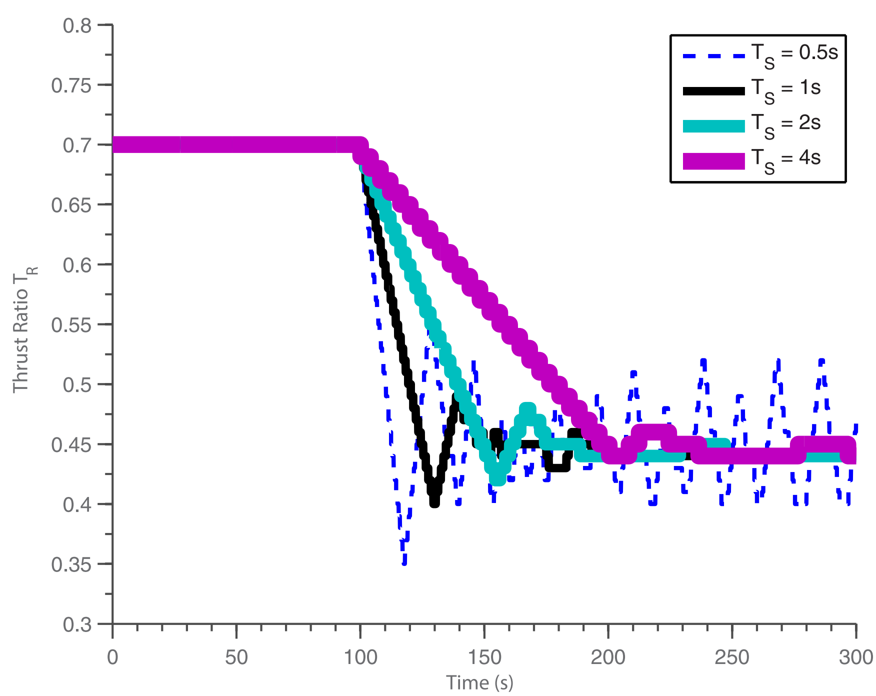

Figure 26. Convergence of thrust ratio for different seeking periods T_S.

Figure 27. The *STARFISH* AUV equipped with a DVL payload and an *in situ* water particle sensing payload.

the thrust ratio. As T_S is increased, the response becomes more stable but the convergence time is longer. $T_S = 1$ s is ideal as it strikes a balance between stability and convergence time. In addition, the results show that the choice of T_S does not affect the optimality.

6. EXPERIMENT RESULTS

We conducted the lake experiments at Pandan Reservoir[5] with the *STARFISH* AUV, equipped with DVL and an *in situ* water particle sensing payload (see Figure 27). The water is considered static and there is no underwater current. Therefore, the AUV speed relative to the surrounding water is equal to its ground speed, which is measured by the DVL.

Figure 28 shows the trajectory of the thrust and speed with respect to time. Initially, the AUV was commanded to cruise at a speed of 1.4 m/s until the seeking algorithm was turned on at 50 s. The thrust ratio was reduced gradually to 0.47 from 0.70. A small transient of T_R was seen in the transition stage. However, the fluctuation was so small that it did not affect the speed, which settled down to 0.75 m/s in 23 s. We observed the same behavior when we compared the experimental results with the simulated ones. The thrust ratio reduced gradually to a minimum point, followed by a small increase, and it settled down quickly thereafter. This similarity attests very strongly to the validity of the model, in the sense that the characteristics of the dynamics are modeled correctly, although the model parameters are not known precisely.

The fact that the thrust ratio settles down to a constant is an appealing feature because this results in a constant speed operation. The settling down of the thrust ratio is not due to the termination of the seeking algorithm. In fact, the algorithm is still active and it will modify the thrust ratio if there is any change in the operating condition. For example, if the AUV experiences a sudden disturbance that affects the pitch error, its speed will be increased to generate more lift to overcome the disturbance. When the disturbance fades away, the seeking algorithm will restore the thrust ratio to its minimum again.

The *STARFISH* AUV is normally operated at a nominal thrust ratio of 0.70, which requires a thrust power of 145 W. If the thrust ratio is reduced to 0.47, the thrust power will be reduced to 43 W, giving a savings of 102 W. If we have 1 kW hour of battery energy for propulsion, traveling at $T_R = 0.47$ instead of 0.70 will increase the vehicle's endurance from 7 to 23 h.[6]

Figure 29 illustrates how the elevator and pitch error evolved with time, and the corresponding FIS output. The data were logged in the seeking algorithm and were only available from 50 s onward. Both the inputs and the FIS output exhibited a similar response to their simulated counterparts. However, since the AUV experienced a disturbance in the real-world environment, the pitch error fluctuated even after the speed had settled down. As a result, the elevator

[5]Pandan Reservoir is located in the western region of Singapore.

[6]For illustration purposes only; the hotel load is not included in the calculation.

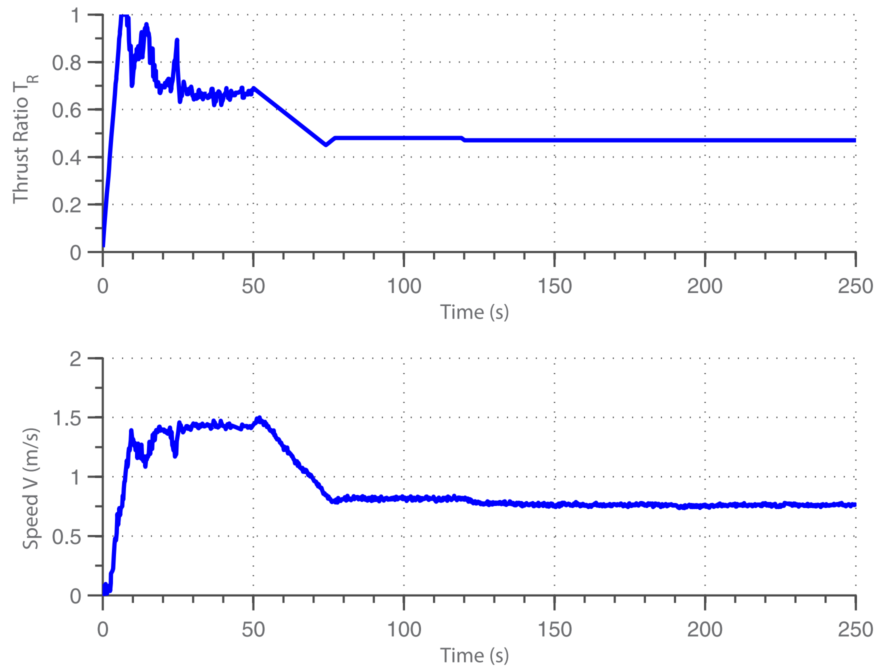

Figure 28. Lake experiment: thrust ratio and speed.

changed rapidly to overcome the disturbance and to keep the pitch error small. Enough fin budget needs to be allocated to counteract the disturbance; otherwise, the pitch error will grow and lead to oscillations in the thrust ratio.

As shown in Figure 30, the AUV pitched at -2° and cruised at 1.4 m/s just before the seeking algorithm was turned on. As the speed was decreased from 50 to 73 s, the pitch angle decreased and settled down to -10°. Throughout the process, the pitch response followed the desired pitch closely. The depth plot shows how the AUV breached the surface and settled down to a 1.5 m depth at 50 s. The depth response displayed a steady-state error because the integral control had not yet been implemented. In other words, the depth controller was a pure proportional controller where steady-state error was expected. Nevertheless, this did not affect the minimum speed seeking algorithm, as depth measurement was not used in the algorithm.

The results that we discussed above are based on experiment 1, in which $\delta_{\max} = 0.26$. We repeated the experiments twice for $\delta_{\max} = 0.35$ and twice for $\delta_{\max} = 0.40$. They are labeled as experiments 2 and 3 and experiments 4 and 5, respectively, as indicated in Table II. Table II summarizes the important vehicle's states, such as depth, pitch angle, thrust ratio, surge speed, heave speed, and elevator deflection, by taking the average of the last 100 s of data (from 150 to 250 s). Their respective standards of deviation are indicated in the parentheses shown underneath their average value.

Let us first look at experiments 2 and 3. They are repeated experiments for $\delta_{\max} = 0.35$. During the steady state, the AUV was pitch at around -12°, traveling at $T_R = 0.44$, with the resultant surge speed around 0.67 m/s for both experiments. This indicates consistency in term of the behavior of the minimum speed seeking algorithm despite working in an unstructured environment that is full of unknown disturbance. Similarly, the results of experiments 4 and 5 for $\delta_{\max} = 0.40$ are also consistent. During the steady state, the AUV was pitched at around -13°, traveling at $T_R = 0.43$, with the resultant surge speed around 0.62 m/s for both experiments. We also overlay the trajectory of thrust ratio and vehicle speed for experiments 2 and 3 and experiments 4 and 5 in Figures 31 and 32, respectively. The results match each other very closely for the repeated experiments.

The results in Table II also show the effect of the fin's effectiveness on the minimum speed. Analysis in Section 3.1 claims that the minimum speed is *inversely* proportional to the fin's effectiveness, and the reduction of the minimum speed is coupled with the decrease of the pitch angle (see also Figure 11). In this case, an increase of $\delta_{\max}$ from 0.26 to 0.40 has a similar effect of increasing the fin's effectiveness, as the $\delta_{\max}$ produces lift force only by multiplication with the fin's effectiveness, $x_f A_f C_{L_\delta}$. The results indicate that the minimum speed decreases and the pitch becomes more negative when $\delta_{\max}$ increases. This matches the theoretical analysis performed in Section 3.1.

When the $\delta_{\max}$ is set to a larger value, the average thrust ratio and hence the average speed are reduced. At the lower speed, the vehicle needs more downward pitching in order to maintain depth, as indicated by the decrease of pitch

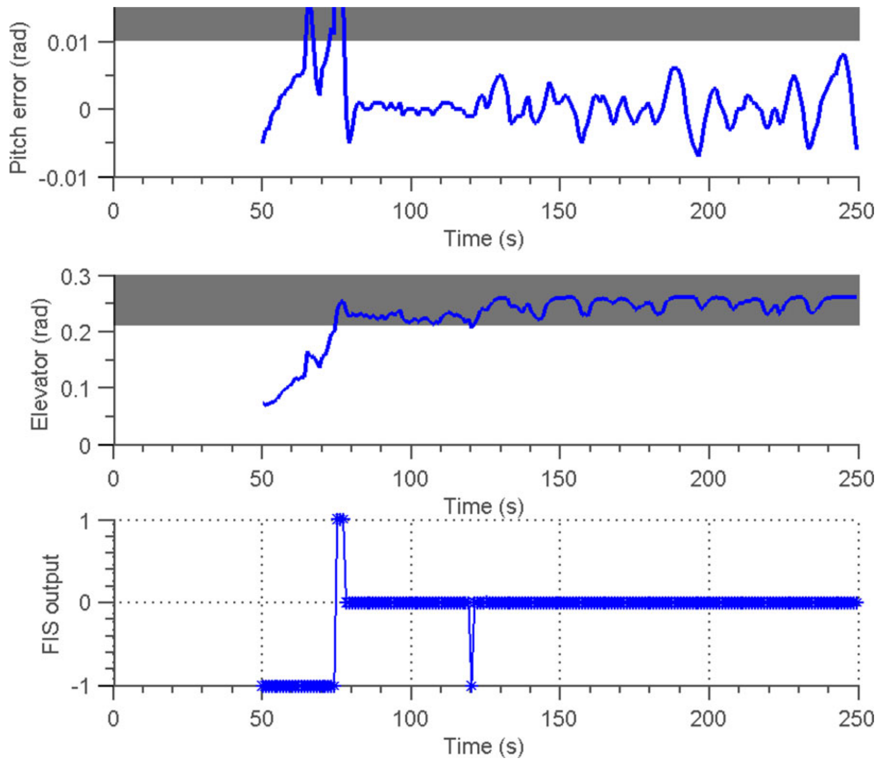

Figure 29. Lake experiment: elevator and pitch error.

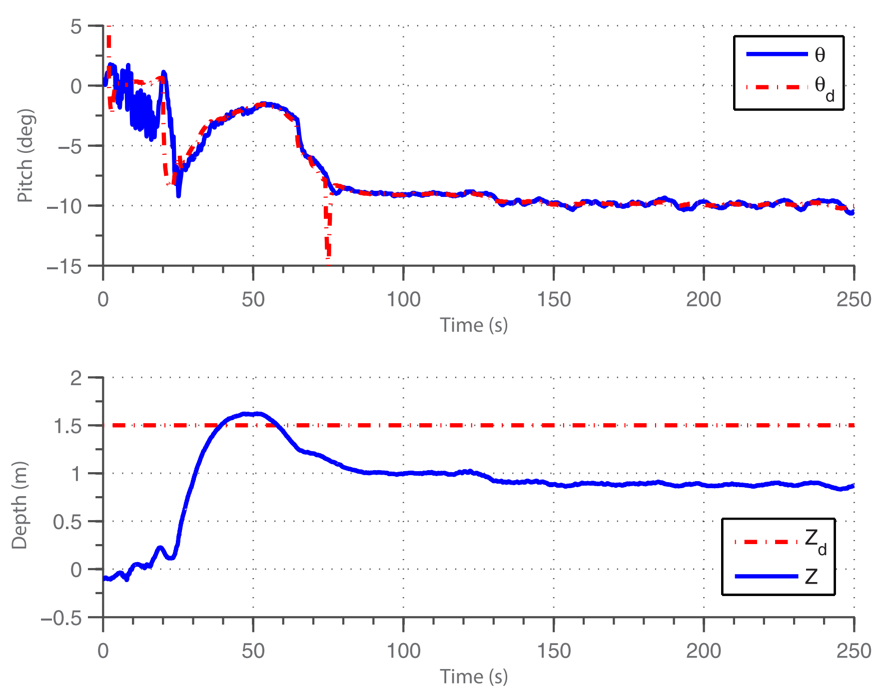

Figure 30. Lake experiment: pitch and depth responses.

Table II. Summary of experimental results during steady state for different δ_{max}.

Experiment No.	δ_{max} (rad)	Depth (m)	Pitch (deg)	T_R	u (m/s)	w (m/s)	δ (rad)
1	0.26	0.89	−9.86	0.47	0.76	−0.14	0.25
		(0.013)	(0.220)	(0.000)	(0.009)	(0.005)	(0.019)
2	0.35	1.10	−12.86	0.44	0.66	−0.16	0.33
		(0.035)	(0.458)	(0.007)	(0.015)	(0.005)	(0.029)
3	0.35	1.22	−11.97	0.44	0.67	−0.15	0.31
		(0.095)	(1.013)	(0.018)	(0.042)	(0.012)	(0.063)
4	0.40	0.91	−13.70	0.43	0.61	−0.16	0.36
		(0.157)	(2.169)	(0.031)	(0.061)	(0.016)	(0.062)
5	0.40	0.80	−13.63	0.43	0.63	−0.16	0.35
		(0.170)	(2.251)	(0.032)	(0.066)	(0.016)	(0.073)

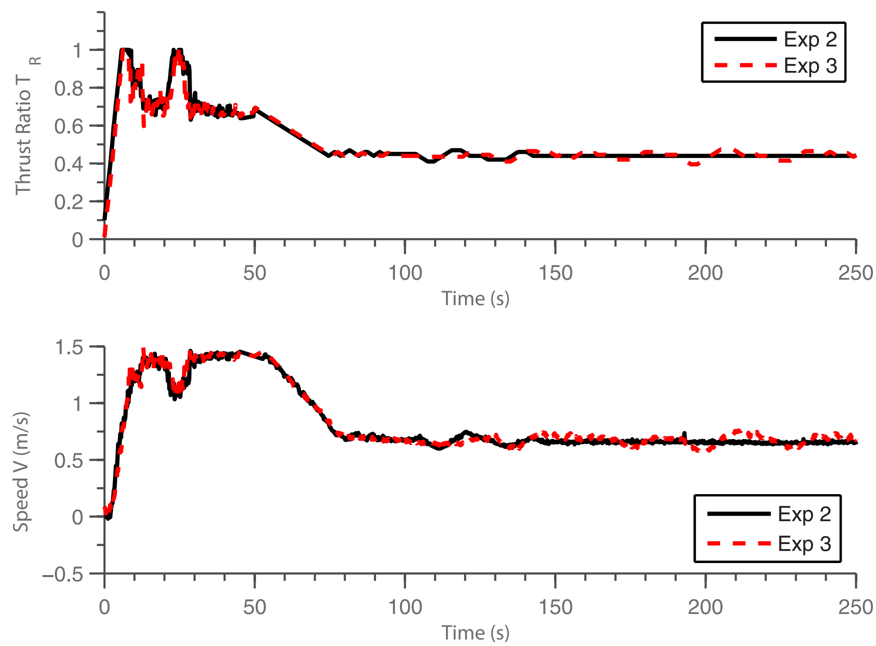

Figure 31. Thrust and speed response for two repeated experiments with $\delta_{max} = 0.35$.

angle. However, for $\delta_{max} = 0.40$, the thrust ratio and the speed of the vehicle are in fact oscillatory, as shown in Figure 32.

The seeking algorithm requires one to know the value of δ_{max}. The value of δ_{max} should have been decided earlier when designing the depth and pitch controller. It is understood that when deciding the value of δ_{max}, controller designers tend to be more conservative to ensure that the fins work within the linear region and away from stall. Here, we investigate the consequence of changing δ_{max} on the optimality of the solution.

We overlay the experiment results for three different δ_{max} in Figure 33. The results show that the gain in thrust deduction is only marginal even though the change in δ_{max} is large (from 0.26 to 0.35). When δ_{max} is set too large, the seeking algorithm will reduce T_R beyond T_R^*. Then, θ_e becomes larger than the θ_e^{TS}, causing the seeking algorithm to increase T_R. When T_R becomes larger than T_R^*, θ_e returns to the normal region. The process repeats itself, forming the limit cycle.

It is of interest to know why the elevator stalls at a much higher value of δ_{max}. As shown in Figure 34, there is a difference between the elevator incidence angle relative to the incoming flow, δ_{se}, and the elevator angle relative to the vehicle hull, δ_s. During a constant depth maneuver, the AUV pitches down at a certain angle β_{se} to maintain depth. This causes the stall to occur at a larger δ_{max}, extended by β_{se}.

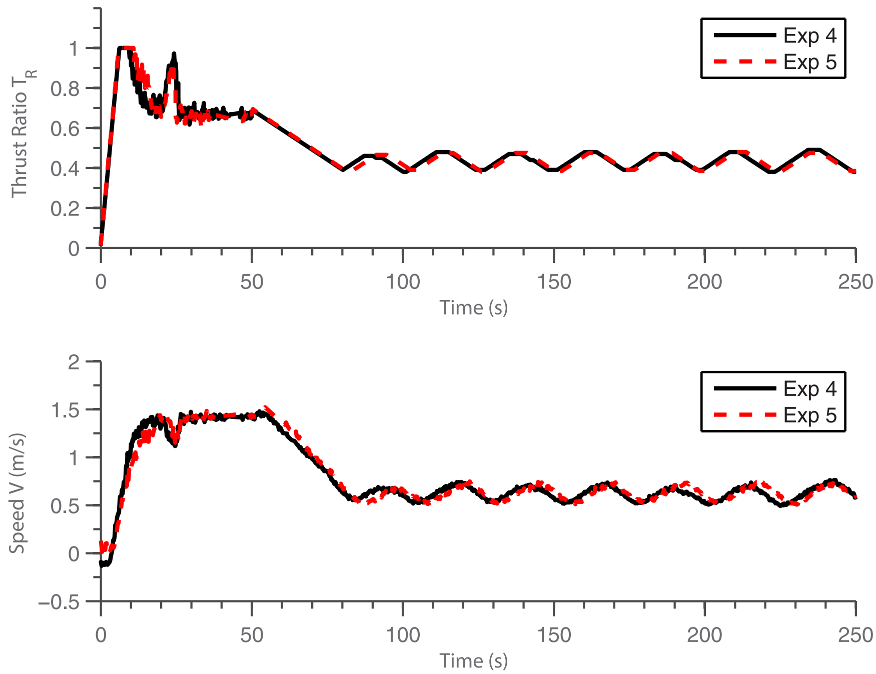

Figure 32. Thrust and speed response for two repeated experiments with $\delta_{max} = 0.40$.

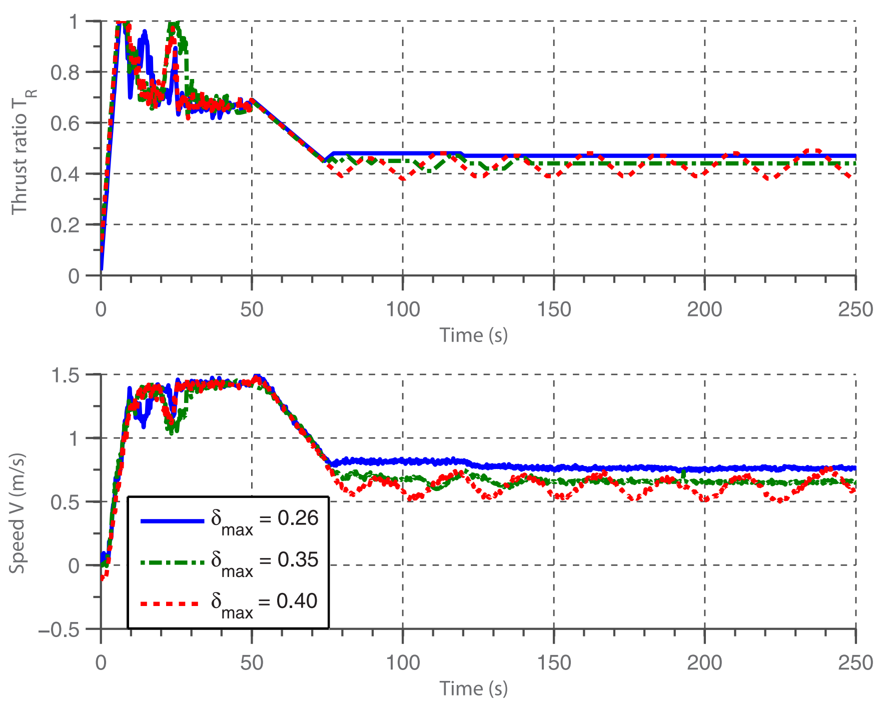

Figure 33. Thrust ratio and speed for different δ_{max}.

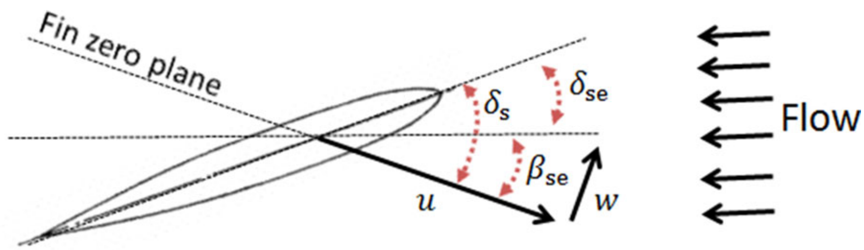

Figure 34. Effective fin angles δ_{se}.

7. CONCLUSION

The need for slow speed AUVs is well documented. Since it is useful for AUVs to move as slowly as possible in some scenarios, we have developed a novel algorithm such that the AUV is automatically controlled to travel at its minimum speed while maintaining a constant depth. While previous research works focused on extending the minimum speed by adding actuators, we propose algorithmic enhancements without the need for any hardware changes. This algorithm is applicable to nonhovering AUVs, which are widely in service nowadays.

First, we construct a depth dynamic model for a typical torpedo-shaped AUV. Through the model, we give the formal definition of the minimum speed. Next, we derive the equations for two important curves: maximum required pitch curve and achievable pitch curve. We then argue that the minimum speed occurs at the intersection of these two curves. The final solution of the minimum speed is then derived together with its condition of existence. By analyzing the maximum required pitch curve and the achievable pitch curve, we study how the buoyancy, righting moment, and the fin's effectiveness affect the minimum speed. This understanding provided us with an insight into how the minimum speed of an AUV could be altered in practice.

However, the model is not useful in predicting the exact value of the minimum speed, as the model's parameters, especially the hydrodynamic coefficients, are not known to have high accuracy. In addition, the minimum speed is also affected by environmental disturbance. Therefore, any prior determination of the minimum speed would be either highly conservative or else it runs the risk of the AUV losing its controllability. A minimum speed seeking algorithm was then developed under the framework of extremum seeking. We fed online measurements of the elevator and the pitch error to a fuzzy inference system, which in turn decided on whether to increase, decrease, or keep the thrust ratio at every seeking interval. The design of the seeking algorithm did not require accurate modeling of the dynamics of the AUV. Instead, the design parameters can be determined based on some known characteristic of the AUV or some available measurements.

The effectiveness of the algorithm in seeking the minimum speed was first studied by simulation. Through simulation, we also investigated the effect of the design parameters on the stability and the optimality of the solution. Next, we verified the seeking algorithm in the lake experiments using the *STARFISH* AUV. The *STARFISH* AUV is normally operated at 0.70 thrust ratio with a nominal speed of 1.4 m/s. The seeking algorithm managed to reduce the thrust ratio to 0.47 with a corresponding speed of 0.75 m/s, while maintaining the depth of the AUV. The seeking algorithm works consistently in a number of repeated experiments.

The effectiveness of the algorithm in seeking the minimum speed of a nonhovering AUV has thus been demonstrated. The availability of such an algorithm as a built-in function of an AUV will open up new possibilities in a number of operation scenarios, such as underwater loitering with minimal energy consumption, underwater docking with minimal impact, and target scanning with minimum speed.

REFERENCES

Abkowitz, M. A. (1969). Stability and motion control of ocean vehicles: Organization, development, and initial notes of a course of instruction in the subject. Cambridge, MA: MIT Press.

Fossen, T. I. (1994). Guidance and control of ocean vehicles. John Wiley & Sons Inc.

Healey, A., & Lienard, D. (1993). Multivariable sliding mode control for autonomous diving and steering of unmanned underwater vehicles. IEEE Journal of Oceanic Engineering, 18(3), 327–339.

Helgason, B. (2012). Low speed modeling and simulation of Gavia AUV. Master's thesis, Reykjavik University.

Jalving, B. (1994). The NDRE AUV flight control system. IEEE Journal of Oceanic Engineering, 19(4), 497–501.

Kongsberg Maritime (2014). Retrieved March 10, 2014, from http://www.km.kongsberg.com/AUV.

Krstić, M., & Wang, H.-H. (2000). Stability of extremum seeking feedback for general nonlinear dynamic systems. Automatica, 36(4), 595–601.

LeBas, P. J. (1997). Maximizing AUV slow speed performance. Master's thesis, Monterey, CA. Naval Postgraduate School.

Liu, J., Furlong, M. E., Palmer, A., Phillips, A. B., Turnock, S. R., & Sharkh, S. M. (2009). Design and control of a flight-style AUV with hovering capability. In, *Proceedings of the International Symposium on Unmanned Untethered Submersible Technology (UUST 2009), Durham, New Hampshire, 23–26 August 2009. UUST 09* Durham NH, USA, Autonomous Undersea Systems Institute (AUSI), [9p].

Nickell, C. L. (2005). Modular modification of a buoyant AUV for low-speed operation. Master's thesis, Virginia Polytechnic Institute and State University.

Nickell, C. L., Woolsey, C. A., & Stilwell, D. J. (2005). A low-speed control module for a streamlined AUV. In Proceedings of MTS/IEEE OCEANS, 2005 (pp. 1680–1685). IEEE.

OceanServer (2014). Retrieved March 10, 2014, from http://iver-auv.com/.

Perumal, L., & Nagi, F. H. (2012). Switching control system based on largest of maximum (lom) defuzzification—Theory and application. Fuzzy Logic–Controls, Concepts, Theories and Applications, InTech, Rijeka (pp. 301–324).

Petrich, J., Neu, W., & Stilwell, D. (2007). Identification of a simplified AUV pitch axis model for control design: Theory and experiments. In IEEE OCEANS 2007 (pp. 1–7).

Petrich, J., & Stilwell, D. (2010). Model simplification for AUV pitch-axis control design. Ocean Engineering, 37(7), 638–651.

Prestero, T. (2001). Verification of a six-degree of freedom simulation model for the REMUS autonomous underwater vehicle. Master's thesis, Massachusetts Institute of Technology and Woods Hole Oceanographic Institution.

R. Benjamin Knapp (2004). Fuzzy sets and pattern recognition. Retrieved March 24, 2014, from http://www.cs.princeton.edu/courses/archive/fall07/cos436/HIDDEN/Knapp/fuzzy 004.htm.

Singh, H., Yoerger, D., & Bradley, A. (1997). Issues in auv design and deployment for oceanographic research. In Proceedings IEEE International Conference on Robotics and Automation 1997, pages 1857–1862 vol.3.

Smith, S. W. (1997). The scientist and engineer's guide to digital signal processing. California Technical Pub., San Diego.

Tan, Y., Moase, W., Manzie, C., Nesic, D., & Mareels, I. (2010). Extremum seeking from 1922 to 2010. In 29th Chinese IEEE Control Conference (CCC) (pp. 14–26).

Teel, A. R., & Popovic, D. (2001). Solving smooth and nonsmooth multivariable extremum seeking problems by the methods of nonlinear programming. In *Proceedings of the American Control Conference, 2001* (vol. 3, pp. 2394–2399).

Teledyne Technologies Incorporated (2014). Retrieved March 10, 2014, from http://www.teledynegavia.com/.

Triantafyllou, M. S., & Hover, F. S. (2002). Maneuvering and control of marine vehicles. Department of Ocean Engineering, Massachusetts Institute of Technology, Cambridge, MA.

Zhang, C., & Ordâoänez, R. (2012). Extremum-seeking control and applications: A numerical optimization-based approach. Springer.